Power-Law Dynamics in Cortical Excitability as probed by Early Somatosensory Evoked Responses

Stephani, T.[1, 2], Waterstraat, G.[3], Haufe, S.[4], Curio, G.[3, 5], Villringer, A.[1, 6, 7], Nikulin, V. V.[1, 8]

[1] Department of Neurology, Max Planck Institute for Human Cognitive and Brain Sciences, Leipzig, Germany

[2] International Max Planck Research School NeuroCom, Leipzig, Germany

[3] Neurophysics Group, Department of Neurology, Charité – Universitätsmedizin Berlin, Berlin, Germany

[4] Berlin Center for Advanced Neuroimaging, Charité – Universitätsmedizin Berlin, Berlin, Germany

[5] Bernstein Center for Computational Neuroscience, Berlin, Germany

[6] Berlin School of Mind and Brain, Humboldt-Universität zu Berlin, Berlin, Germany

[7] Clinic for Cognitive Neurology, University Hospital Leipzig, Leipzig, Germany

[8] Center for Cognition and Decision Making, National Research University Higher School of Economics, Moscow, Russian Federation

Abstract

While it is well-established that instantaneous changes in neuronal networks´ states lead to variability in brain responses and behavior, the mechanisms causing this variability are poorly understood. Insights into the organization of underlying system dynamics may be gained by examining the temporal structure of network state fluctuations, such as reflected in instantaneous cortical excitability. Using the early part of single-trial somatosensory evoked potentials in the human EEG, we non-invasively tracked the magnitude of excitatory post-synaptic potentials in the primary somatosensory cortex (BA 3b) in response to median nerve stimulation. Fluctuations in cortical excitability demonstrated long-range temporal dependencies decaying according to a power-law across trials. As these dynamics covaried with pre-stimulus alpha oscillations, we establish a functional link between ongoing and evoked activity and argue that the co-emergence of similar temporal power-laws may originate from neuronal networks poised close to a critical state, representing a parsimonious organizing principle of neural variability.

1 Introduction

Evoked brain responses demonstrate remarkable variability even when they are produced by the same stimulus. This observation is ubiquitous for diverse neuronal measures, such as EEG (Forschack, Nierhaus, Müller, & Villringer, 2017; Iemi et al., 2019; Jansen & Brandt, 1991; Rahn & Basar, 1993; Romei et al., 2008; Vanrullen, Busch, Drewes, & Dubois, 2011), BOLD signal (Becker, Reinacher, Freyer, Villringer, & Ritter, 2011; Fox & Raichle, 2007), LFP (Arieli, Sterkin, Grinvald, & Aertsen, 1996), and single-cell recordings (Azouz & Gray, 1999; Churchland et al., 2010). Furthermore, the variability in neuronal activity is linked to variability in behavioral responses (Britten, Newsome, Shadlen, Celebrini, & Movshon, 1996; Dinstein, Heeger, & Behrmann, 2015; Renart & Machens, 2014), thus emphasizing the importance to understand its mechanisms in more detail.

It has been proposed that variability in brain responses originates from fluctuations in the instantaneous brain state (Arieli et al., 1996; Sadaghiani, Hesselmann, Friston, & Kleinschmidt, 2010) which can in turn be associated with changes of cortical excitability, as has been suggested particularly for alpha band activity (8-12 Hz) in the EEG (Jensen & Mazaheri, 2010; Klimesch, Sauseng, & Hanslmayr, 2007; Mathewson et al., 2011). On the one hand, trial-to-trial variability of cortical excitability posits a major challenge for research on stimulus-related brain processes, as typically only responses averaged over many trials can be investigated, and these averages do not necessarily reflect the actual brain processes on a single-trial level. On the other hand, as we will show here, investigating the dynamics of this neuronal variability offers a unique opportunity to gain deeper insights into the complex spatio-temporal organization of the neuronal system.

So far, studies on neuronal variability have mainly focused on the *strength* of variability (Dinstein et al., 2015; Garrett et al., 2013), comparing, for example, the extent of pre- and post-stimulus variability (Churchland et al., 2010). The *nature* or *type* of neuronal variability, however, has often been neglected although it may reveal even more details of the mechanisms

underlying the neuronal variability. On a conceptual level, three different types of variability can be distinguished in neural signals regarding their temporal dynamics (Fig. 1).

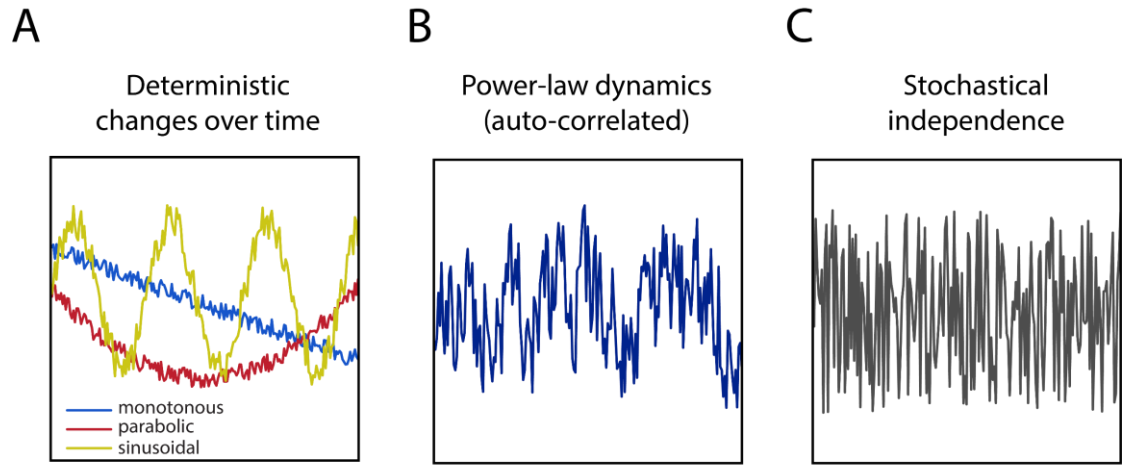

Fig. 1. Types of signal variability. A) Deterministic changes. B) Partially deterministic changes, i.e. power-law dynamics (auto-correlated). C) Stochastically independent fluctuation (completely indeterministic).

First, a measure of interest can show a deterministic change over time. This can be a monotonous de- or increase or another regular pattern, such as a sinusoidal or parabolic signal change. For example, habituation processes may lead to a monotonous decrease of neural responses to identical stimuli presented repeatedly (i.e., repetition suppression; Grill-Spector, Henson, & Martin, 2006). Second, the signal may not show any deterministic pattern but fluctuate stochastically independently (i.e., "white noise"). In this case, the data does not show any temporal pattern and there is no relationship between the samples of the signal. This type of variability is, for example, often used as an assumption in modeling approaches of physiological time series (Richman & Moorman, 2000). Besides these two common types of variability, a third class has recently received much attention, so-called *power-law dynamics*, which seem to play an important role in the (self-)organization of complex biological systems (Muñoz, 2018; Sethna, Dahmen, & Myers, 2001). For this type of variability, the samples of

the signal are not independent and show long-lasting temporal dependencies. Thus, the signal is partially but not entirely deterministic. Characteristically, the fluctuation of such a signal is related to the length of the data according to a power-law: $F(\tau) \propto \tau^{\alpha}$, where F is the cumulative fluctuation, τ is the signal length (or window size), and α the power-law exponent. Signals following such a power-law have also been termed as *scale-free* or *self-similar* as their statistical properties are similar on micro-, meso-, and macroscale. Importantly, it has been shown that complex systems that are poised at the phase transition between two distinct states, such as order and disorder, typically show power-law dynamics both in their spatial and temporal dynamics (Sethna et al., 2001). This phase transition has been referred to as the so-called *critical state* (Bak, Tang, & Wiesenfeld, 1987; P. Bak, Tang, & Wiesenfeld, 1988; Beggs & Plenz, 2003). Figure 2A visualizes the described system states using the *Ising model of ferromagnetism* (Ising, 1925), a model of temperature-dependent spontaneous transitions between magnetization states in ferromagnetic material, which has also been successfully used to model complex neuronal dynamics (Botcharova, Farmer, & Berthouze, 2014; Kitzbichler, Smith, Christensen, & Bullmore, 2009; Schneidman, Berry II, Segev, & Bialek, 2006; Sethna et al., 2001).

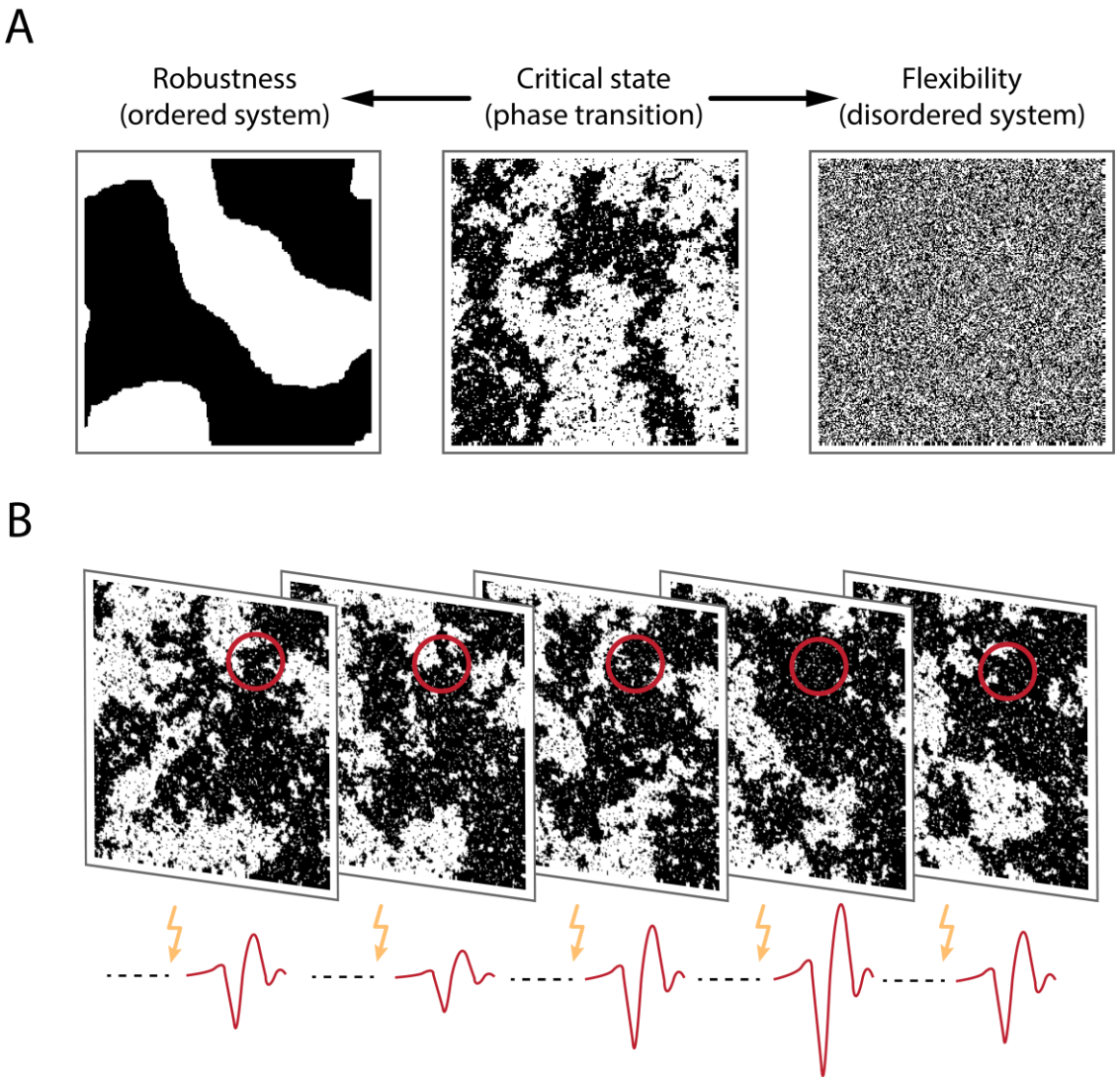

Fig. 2. A) *Ising model* at different system states: ordered, critical, disordered (from left to right). Transferred to a grid of neurons, black and white color reflect firing and non-firing neurons, respectively. Here, snapshots of the system at a given time point are shown. In an ordered system, local interactions dominate and lead to highly stable neural activity. In contrast, firing patterns in a disordered system are very unstable and change fast from moment to moment in a stochastically independent manner (i.e., white noise). At the critical state, the system resides at the border between the tendencies either towards an ordered or towards a disordered system. This is reflected by the spatio-temporal dynamics, that is, scale-invariance or power-law dynamics. Scale-invariance is visible from the middle panel as similar clusters of black pixels occur on all scales. B) Experimental paradigm. The instantaneous state of the neuronal system (here illustrated with snapshots from the Ising model at the critical state) is probed using somatosensory stimuli. SEP fluctuations should directly reflect dynamics of the instantaneous system state since evoked responses with amplitude A are approximately proportional to the number of synchronously recruited neurons, formally written as $A(N) \sim cN$, where c depends on the leadfield matrix properties and N reflects the number of neurons capable of generating a response (black pixels which are in the probed area, indicated by the red circle). In a stable system, the number of neurons N would barely change over time whereas in an unstable system N would be random. Yet at the critical state, N would show the largest range of variation over time.

In neuronal systems, criticality seems to be a general organization principle reflecting a dynamic equilibrium between coordinated (ordered) and uncoordinated (disordered) neuronal activity: Power-law dynamics indicating proximity to the critical state have been found in the size and duration of neuronal avalanches in rat brain slices (Beggs & Plenz, 2003; Friedman et al., 2012), monkeys (Petermann et al., 2009; Priesemann, Munk, & Wibral, 2009; Yu et al., 2017), cats (Hahn et al., 2010), zebrafish larvae (Ponce-Alvarez, Jouary, Privat, Deco, & Sumbre, 2018), as well as humans (Arviv, Goldstein, & Shriki, 2015; Priesemann, Valderrama, Wibral, & van Quyen, 2013; Shriki et al., 2013). Furthermore, when focusing on the temporal domain, power-law dynamics can be found in human resting-state fMRI networks (Tagliazucchi et al., 2013), as well as in amplitude fluctuations of alpha band activity in the MEG (Linkenkaer-Hansen, Nikouline, Palva, & Ilmoniemi, 2001; Palva et al., 2013). In addition, a recent study observed that even single-cell membrane potentials in the turtle visual cortex show critical dynamics (Johnson, Wright, Xia, & Wessel, 2019). These findings suggest that fluctuations of the instantaneous brain state are characterized by a complex spatio-temporal structure, leading to endogenous dynamics in cortical excitability which, in turn, should affect the commonly observed variability in brain responses, such as ERPs. However, the link between power-law dynamics of instantaneous brain states, cortical excitability, and fluctuation of brain responses in the human brain is still elusive, and evidence for such a temporal structure in human ERPs is still missing.

To test this relationship, a direct measure of cortical excitation is needed, ideally manifested in a well-defined neuronal process. Whereas previous studies proposed that alpha band activity reflects cortical excitability (Klimesch et al., 2007; Pfurtscheller, Stancák, & Neuper, 1996; Romei et al., 2008), its mechanistic underpinnings are still under debate (van Diepen, Foxe, & Mazaheri, 2019), and the modulatory role of alpha activity seems to be more pronounced for higher-level cognitive processes, such as perceptual confidence (Samaha, Iemi, & Postle, 2017), rather than for excitability on a more basic, neurophysiological level.

Here we propose an alternative, more direct measure of instantaneous cortical excitability based on somatosensory evoked potentials (SEP) in response to median nerve stimulation, measured non-invasively with EEG.

Specifically, the N20 component of the SEP is thought to solely reflect excitatory post-synaptic potentials (EPSPs) of the first thalamo-cortical volley (Bruyns-Haylett et al., 2017; Nicholson Peterson, Schroeder, & Arezzo, 1995; Wikström et al., 1996), generated in the anterior wall of the postcentral gyrus, Brodmann area 3b (Allison, McCarthy, Wood, & Jones, 1991). Recent evidence from pharmacological studies furthermore suggests that excitatory processes dominate even until the rising flank of the P35, the next component after the N20 in the SEP (Bruyns-Haylett et al., 2017). Therefore, the amplitude of this early part of the SEP represents a direct probe of the instantaneous excitability of a well-defined neuron population in the somatosensory cortex.

In the present study, we probed the excitability of the primary somatosensory cortex in humans using electrical median nerve stimuli and investigated its variability over time with single-trial SEP amplitudes in the EEG (Fig. 2B). The temporal structure of excitability changes was examined using Detrended Fluctuation Analysis (DFA; Hardstone et al., 2012; Kantelhardt, Koscielny-Bunde, Rego, Havlin, & Bunde, 2001). Indeed, while controlling for subcortical and peripheral signal variability, we found power-law dynamics in early cortical SEPs over trials. Thus, fluctuations of cortical excitability in the primary somatosensory cortex were characterized by long-range temporal dependencies, consistent with the hypothesis that cortical network dynamics are poised at a critical state. In addition, pre-stimulus alpha band activity and initial cortex excitation, as reflected in the N20 component, demonstrated a close relationship as both their amplitudes and temporal structure (i.e., power-law dynamics) were coupled. Hence, similar network mechanisms may govern variability in both ongoing and evoked neural activity.

2 Results

SEPs and neuronal generators

The SEPs, averaged across all participants and trials, are shown in Figure 3. As expected, a negative peak at around 20 ms and a positive peak at around 35 ms are visible in the electrodes contralateral to the stimulation site and posterior to the central sulcus. Furthermore, the scalp topography at 20 ms shows a typical dipole pattern consistent with the assumption of neuronal generators located in the anterior wall of the postcentral gyrus.

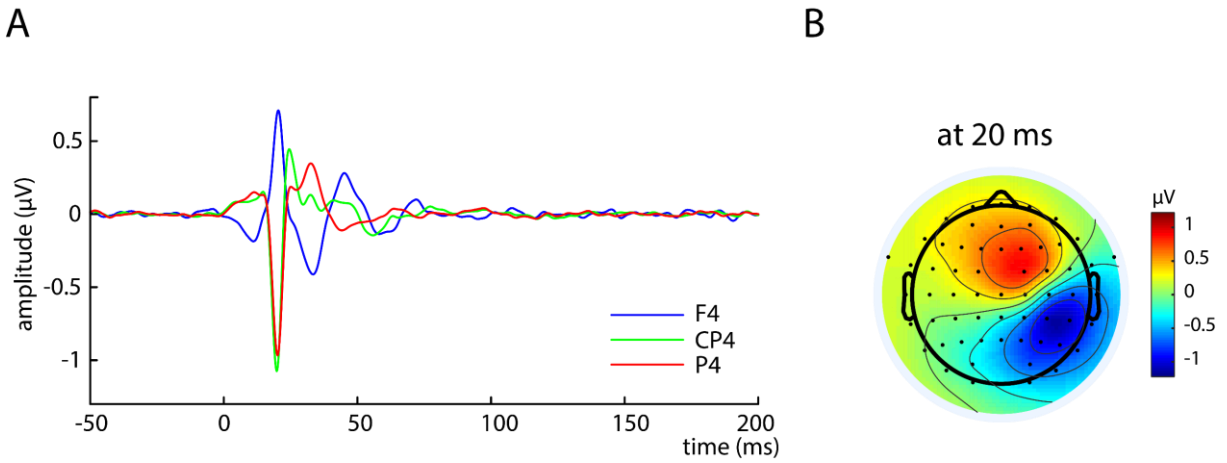

Fig. 3. Grand average of SEPs across all subjects in sensor space. A) Somatosensory evoked potential (SEP) at F4 (blue), CP4 (green), and P4 (red). B) Scalp topography at 20 ms post-stimulus.

To extract single-trial SEPs we used a variant of Canonical Correlation Analysis (CCA) in which spatial filters were trained based on a pattern matching between average SEP and single trials (Fedele et al., 2013; Waterstraat, Fedele, Burghoff, Scheer, & Curio, 2015). With this method, we obtained a set of spatially distinct CCA components for every individual subject. In all subjects, a prominent CCA component was identified that displayed a pattern consistent with a tangential dipole centered over the central sulcus, as it would be expected for generators located in the anterior wall of the postcentral gyrus (Fig. 4A).

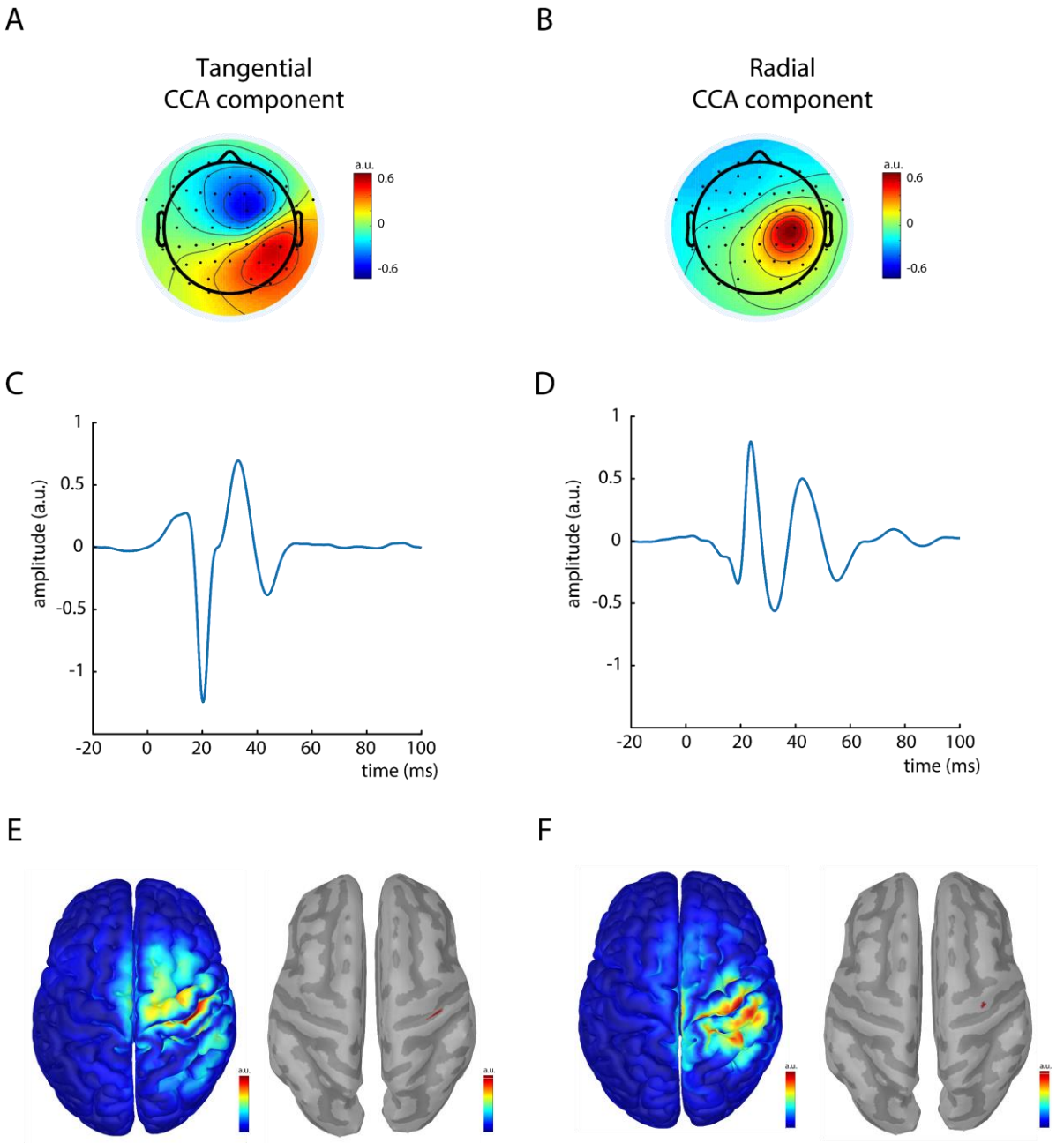

Fig. 4. Categorization of CCA components into a tangential and a radial component. Panels A and B show the spatial patterns, panels C and D the activation time courses of the tangential and radial component, respectively. Panels E and F depict sources (absolute values) underlying the spatial patterns of the tangential and radial component, respectively, reconstructed using eLoreta based on models of individual brain anatomies; left sub-panels without threshold, right panels thresholded at 95% amplitude. All panels (A to F) depict averages across participants and trials.

In addition, in most subjects another CCA component was consistently found that was characterized by a radial pattern (Fig. 4B). In all subjects, these two spatially distinct CCA components were among the first three most prominent CCA components (i.e., highest correlation with the SEP average; see methods section for more details). In the temporal domain,

the tangential CCA component showed a large negative peak at around 20 ms post-stimulus (Fig. 4C) whereas the radial component´s activity seemed to be more pronounced slightly later at around 25 ms (Fig. 4D). Moreover, subsequent source reconstruction of the spatial patterns indeed showed that the strongest generators of the tangential component were located in the anterior wall of the postcentral gyrus (Fig. 4E) whereas generators of the radial component tended to be on top of pre- and post-central gyri (Fig. 4F). Both the temporal as well as the spatial characteristics suggest that the tangential CCA component reflected activity related to the N20 component of the SEP, associated with the initial cortex excitation. In the following analyses, we therefore focus on the tangential CCA component.

Single-trial SEPs retrieved for the tangential CCA component are displayed in Figure 5A for an exemplary subject. It is apparent that the amplitude of the early SEP fluctuates over trials, however without a clear monotonous trend (Figure 5B).

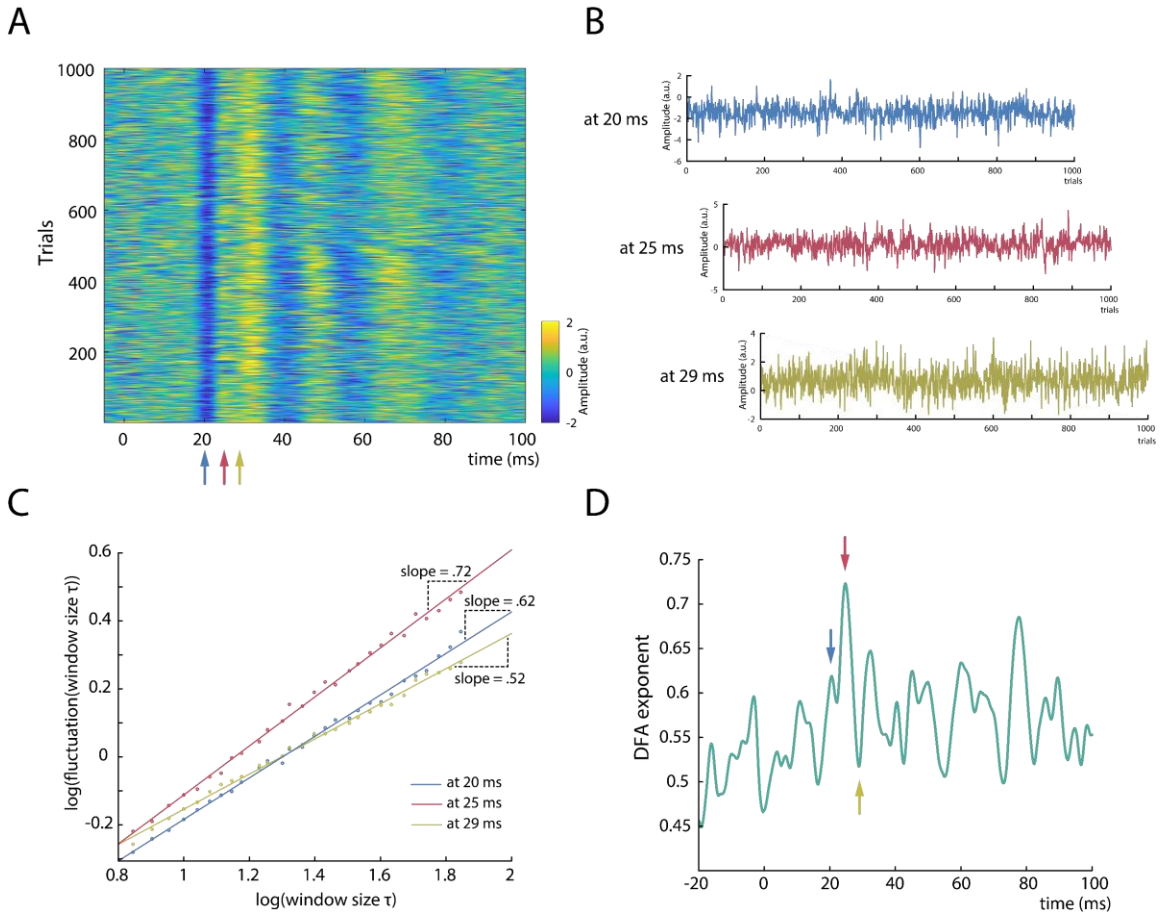

Fig. 5. Analysis of power-law dynamics in SEP amplitude fluctuations for an exemplary subject. A) Single-trial SEPs extracted using CCA; depicted is the tangential CCA component. B) SEP amplitude fluctuations across trials for exemplary latencies (20 ms, 25 ms, and 29 ms post-stimulus). C) Detrended Fluctuation Analysis (DFA) for amplitude fluctuations depicted in B. Indicated slopes reflect the respective DFA exponents quantifying the power-law dynamics of the signal. D) Time course of DFA exponents in an exemplary subject; blue, red, and yellow arrows mark the latencies which are displayed in B and C.

Temporal dynamics in single-trial SEP amplitude fluctuations

To evaluate the characteristics of SEP fluctuations across trials, we applied Detrended Fluctuation Analysis (DFA). The DFA exponent α quantifies the extent of power-law dynamics of a signal, with $\alpha > 0.5$ indicating persistent auto-correlations; whereas $\alpha = 0.5$ would suggest a signal without a temporal structure (i.e., white noise). DFA was performed on the amplitudes at every latency relative to the stimulus onset, across trials. Figure 5C depicts the DFAs for the three exemplary amplitude time series from Figure 5B, measuring the power-law exponent α as

the slope of a regression line fitted to the log-log relationship between window size τ and the fluctuation of each window size. Applying DFA at all latencies provided a *DFA exponent time course* for every subject (Fig. 5D). This time course indicates which portions of the early SEP show power-law dynamics (i.e., DFA exponents > 0.5) and thus do not fluctuate stochastically independently across the trials. Subsequently, DFA exponent time courses were averaged across participants. The average explained variance of the power-law relationship between window size τ and the fluctuation within a given window of size τ was $R^2 > .99$ at all latencies in the time range of the early SEP (10 and 50 ms), indicating a near-perfect fit of the DFA method for this data.

Increased DFA exponents were observed particularly in the early part of the SEP whereas surrogate data generated by shuffling the trial order yielded DFA exponents close to $\alpha = 0.5$ (Fig. 6A). Two prominent peaks in the DFA exponent time course are visible from Figure 6B, with DFA exponents of $\alpha = .575$ and $\alpha = .577$, at latencies of 25 and 33 ms post-stimulus, respectively. Note, however, that the absolute value of DFA exponents highly depends on the signal-to-noise ratio (SNR) of the signal, as is further examined in simulations below which suggest DFA exponents of at least $\alpha = .63$ when the SNR bias is taken into account. The observation of two prominent DFA exponent peaks was statistically confirmed as two main clusters were found around these two peaks by cluster-based permutation tests ($ps_{cluster} < .001$), the first cluster starting at around the latency of the N20 component. Interestingly, the DFA exponents were characterized by a similar yet not identical time course as compared to the magnitude of the SEP (Fig. 6B). The second DFA exponent cluster peaked at around the same latency as the P35 component of the SEP whereas the first DFA cluster peaked at around 25 ms, thus slightly later than the N20 component. Temporal filtering in the preprocessing of the data cannot have caused these long-range temporal dependencies since no DFA exponent increases were observed during the pre-stimulus baseline of the SEP, and additional control analyses did

not show increased DFA exponents when applying the same preprocessing to stochastically independent SEP fluctuations (simulated data).

Additionally, we examined the relationship between single-trial N20 and P35 peak amplitudes using a random-slope linear-mixed-effects model with *P35 peak amplitude* as dependent variable, *N20 peak amplitude* as independent variable and *subject* as random factor. Across subjects, we found a moderate negative relationship between N20 and P35, β_{fixed} = -.378, $t(29.800)$ = -9.342, $p < .001$ (fixed effect of *N20 peak amplitude* on *P35 peak amplitude*).

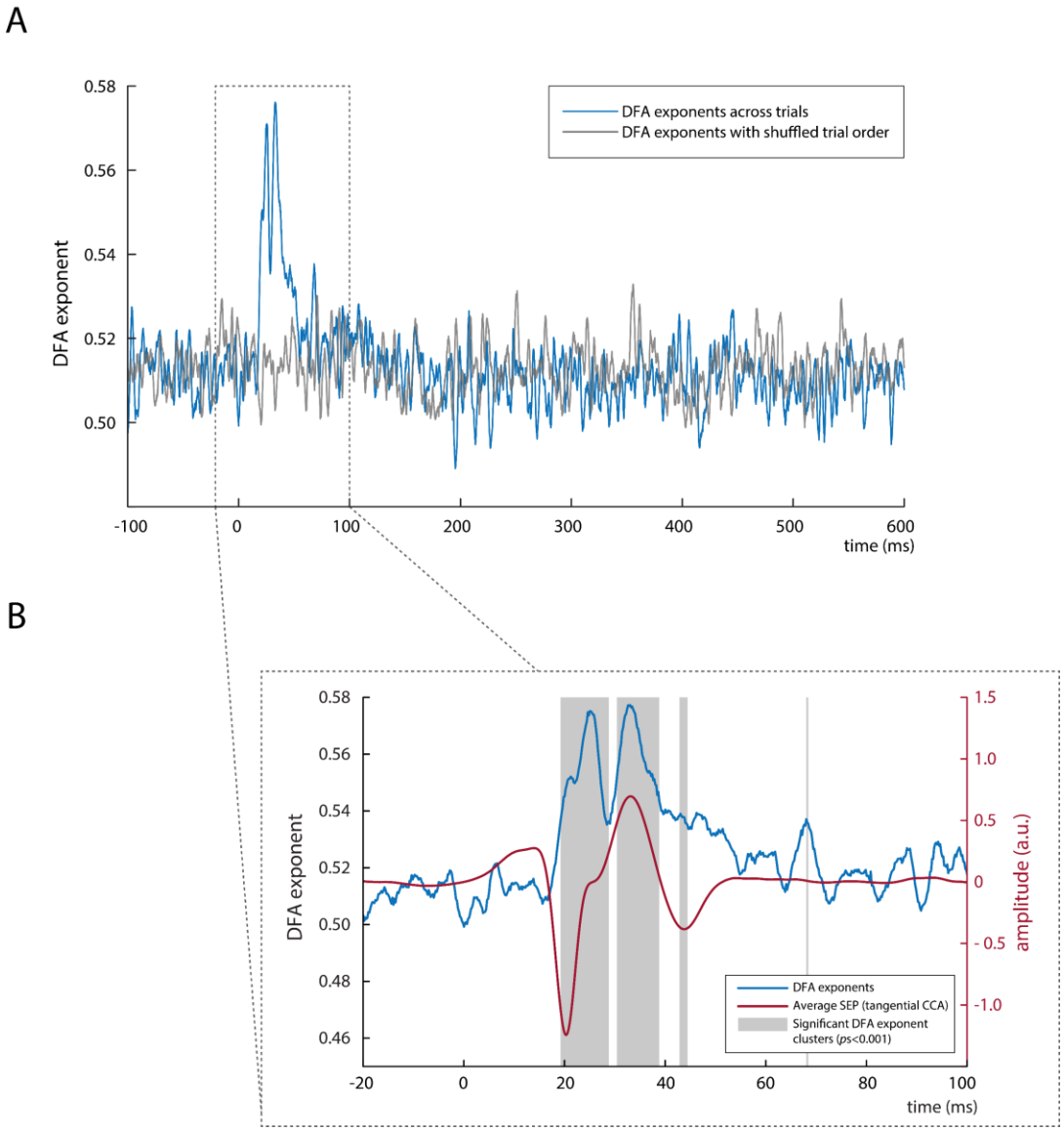

Fig. 6. A) Time course of DFA exponents calculated for SEP fluctuations across trials (blue), and DFA exponents of surrogate data (shuffled trial order; grey); both averaged over participants. B) Enlarged view of DFA exponents (blue) in the range of the earliest SEP components (red). Grey boxes indicate significant clusters of DFA exponents significantly differing from $\alpha = 0.51$ (i.e., average DFA exponent with shuffled trial order).

Do power-law dynamics originate from the neuronal fluctuations in the periphery or at the thalamic level?

To investigate whether the observed temporal dynamics in cortical SEPs may arise from fluctuations in the peripheral nerve excitability, we applied the same procedure as described above to the compound nerve action potential (CNAP) of the median nerve measured at the inner side of the upper arm. As expected, the nerve potential peaked at around 6 ms post-stimulus and fluctuated over trials (Fig. 7A). However, no increased DFA exponents were observed (Fig. 7B).

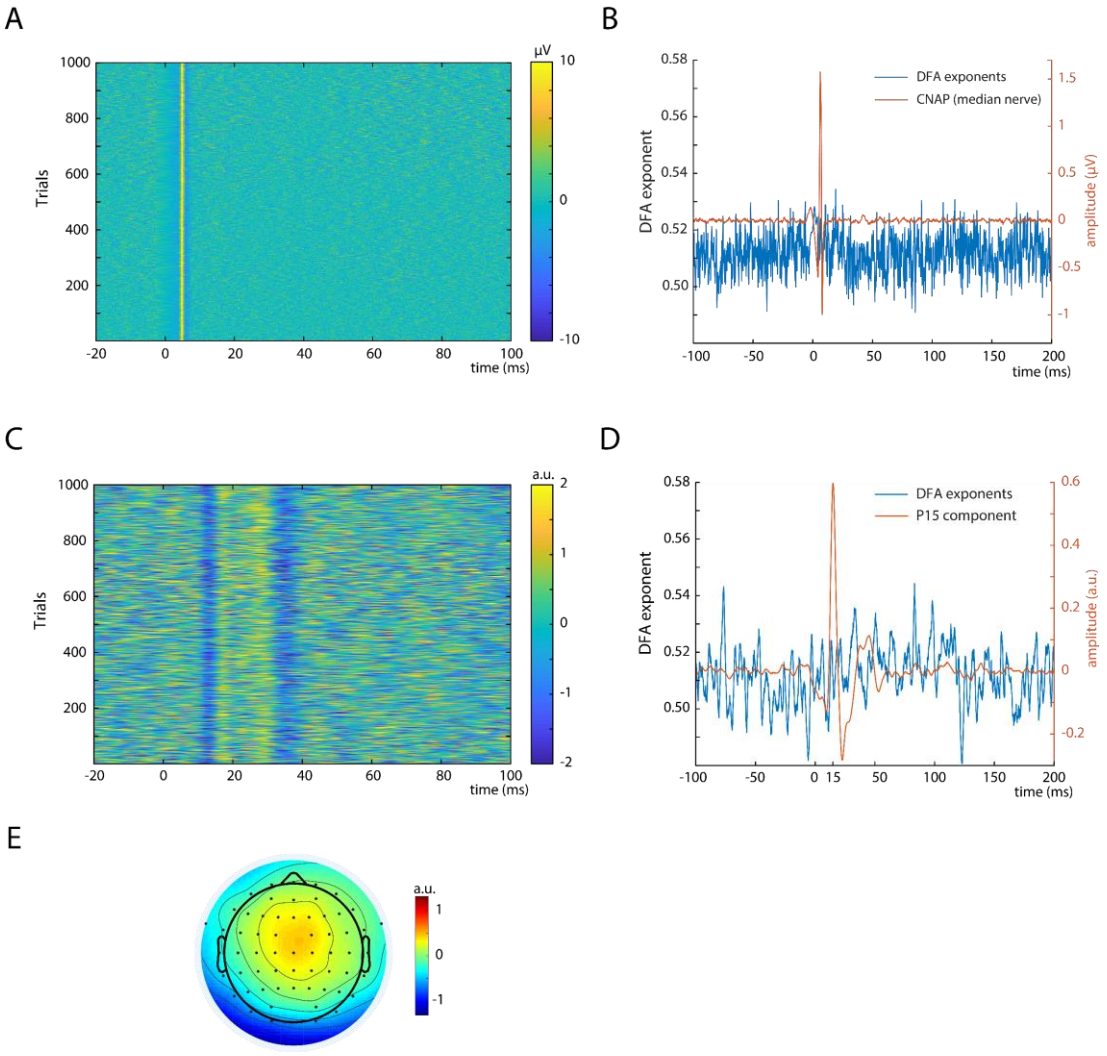

Fig. 7. Control measures. A) Single-trial compound nerve action potentials (CNAP) of the median nerve measured on the inner side of the upper arm; depicted for an exemplary subject. B) DFA exponents (blue) and CNAP (orange) of the median nerve; averaged over all subjects. C) Single-trial SEPs of the thalamus-related CCA component of an exemplary subject. D) DFA exponents (blue) and SEP (orange) of the thalamus-related CCA component; averaged over the 13 subjects in which a peak at around 15 ms was observed on single-trial level. E) Average spatial pattern of the thalamus-related CCA components; averaged over 13 subjects.

In addition, a CCA component was identified in 13 out of the 31 participants that contained SEP activity already at 15 ms (Fig. 7C & 7D), most likely reflecting the P15 component of the SEP which is thought to represent thalamus-related activity (Albe-Fessard, Tasker, Yamashiro, Chodakiewitz, & Dostrovsky, 1986). Also, the spatial patterns of this CCA component suggested a deeper and more medial source than the tangential or radial CCA components (Fig. 7E). Importantly, the DFA exponents of this subcortical activity did not show any increase in the range of the P15 component (Fig. 7D) thus being in contrast with the DFA exponent increase for early cortical potentials.

DFA exponents and SNR

Since it is known from previous studies that the signal-to-noise ratio (SNR) highly affects the measurement of power-law dynamics (Blythe, Haufe, Müller, & Nikulin, 2014), we investigated the relationship between DFA exponents and SNR in single-trial SEPs. On average across all participants, the SNR of the tangential CCA component was $\frac{rms(signal)}{rms(noise)} = 1.68$ (SD = .42), and showed a positive rank correlation with DFA exponent increase in the time range from 10 to 50 ms post-stimulus, $r = .36$, $p = .049$.

Additionally, we further clarified this relationship with simulations: We mixed signals expressing different DFA exponents with white noise (DFA exponent $\alpha = 0.5$), for a range of SNRs, and measured the DFA exponent of these mixed signals. As is visible from Figure 8, DFA exponents of the mixed signals are attenuated towards $\alpha = 0.5$ when lowering the SNR. Given an SNR of 1.68 and an empirical DFA exponent of $\alpha = 0.575$, as was the case for the tangential CCA component in the present study, our simulations suggest an underlying source with a DFA exponent of $\alpha \approx 0.63$.

To relate this simulation also to the others measures for which we calculated DFA exponents, we calculated the SNR of the CNAP at the upper arm and thalamic CCA components. Here, we found SNRs of 2.20 (SD = .85) and 1.33 (SD = .11), respectively, suggesting that our

signal quality was sufficient to detect DFA exponent increases if they had been there since the SNR of the CNAP was even higher than that of the SEP and the SNR of the thalamic CCA component was just slightly lower.

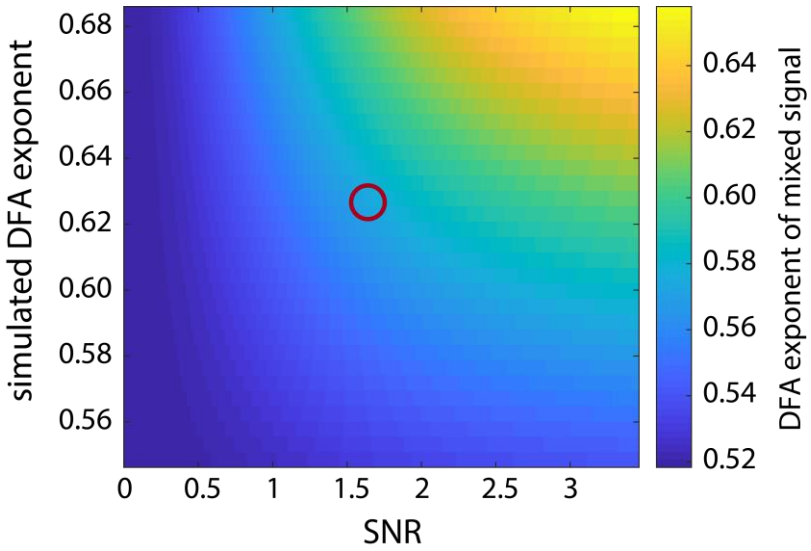

Fig. 8. Simulation of the influence of signal-to-noise ratio (SNR) on the measurement of DFA exponents. Signals with varying DFA exponents (plotted on vertical axis) were mixed with white noise (i.e., DFA exponents of ~0.5) with varying SNR (plotted on horizontal axis). The resulting DFA exponents of the mixed signals are color-coded. The red circle indicates the region of empirically observed DFA exponents of ~0.57 at an SNR of ~1.68 suggesting an underlying DFA exponent of the unmixed source of ~0.63.

Power-law dynamics in alpha band activity and its relation to the SEP

Since previous studies on cortical excitability in M/EEG focused on oscillatory activity in the alpha band, we investigated both its correspondence to the early part of the SEP as well as its DFA exponents.

To test the relationship between alpha oscillatory activity and SEP amplitude, we performed a regression analysis between the mean alpha amplitude in a pre-stimulus window from -200 to -10 ms and the peak amplitude of the N20 component. Alpha activity was extracted from the same neuronal sources as the SEP by applying the spatial filter of the tangential CCA component. A significant negative relationship was found on group-level using a random-slope linear-mixed-effects model, β_{fixed} = -.034, $t(25.689)$ = -4.984, p < .001. Thus, higher pre-

stimulus alpha activity was associated with more negative N20 peak amplitudes. To control for spurious covariation caused by the auto-correlated structure of both signals, we additionally ran permutation tests using surrogate data with comparable temporal structure as suggested in Schaworonkow, Blythe, Kegeles, Curio, and Nikulin (2015). Aggregated on group-level, these tests confirmed the negative relationship between pre-stimulus alpha activity and N20 peak amplitude, $r_{\text{group-level}} = -.035$, $p < .001$.

Next, we investigated the DFA exponents of mean pre-stimulus alpha amplitude across trials. Averaged across subjects, we observed a mean DFA exponent of $\alpha = .60$, which significantly differed from DFA exponents for shuffled trial order, $t(30) = 6.627$, $p < .001$. Also, DFA exponents in continuous, ongoing alpha activity were significantly increased across subjects, $\alpha = .66$, $t(30) = 10.591$, $p < .001$. Thus, power-law dynamics were present in both pre-stimulus and continuous, ongoing alpha activity.

To further test the relationship between pre-stimulus and SEP dynamics, we correlated DFA exponents of pre-stimulus alpha amplitude and DFA exponents of the SEP across participants. DFA exponents of the SEP were aggregated (using root-mean-square) in four consecutive time windows of 5 ms each, between 20 and 40 ms post-stimulus. DFA exponents of alpha activity were correlated with the DFA exponents of the first time window from 20 to 25 ms, $r = .485$, $p = .025$ (Bonferroni-corrected). However, this relationship did not emerge for any other time window between 25 and 40 ms, ps > .3 (Fig. 9). Notably, the SNR of the SEP cannot explain the relation between DFA exponents of alpha activity and DFA exponents of the SEP, as no relationship was found between SNR of the SEP and DFA exponents of pre-stimulus alpha activity, $r = .208$, $p = .261$.

Taken together, our results show that both amplitude and temporal structure of oscillatory activity in the alpha band relate to the corresponding parameters of the early SEP responses, establishing a link between these two measures of instantaneous cortical excitability.

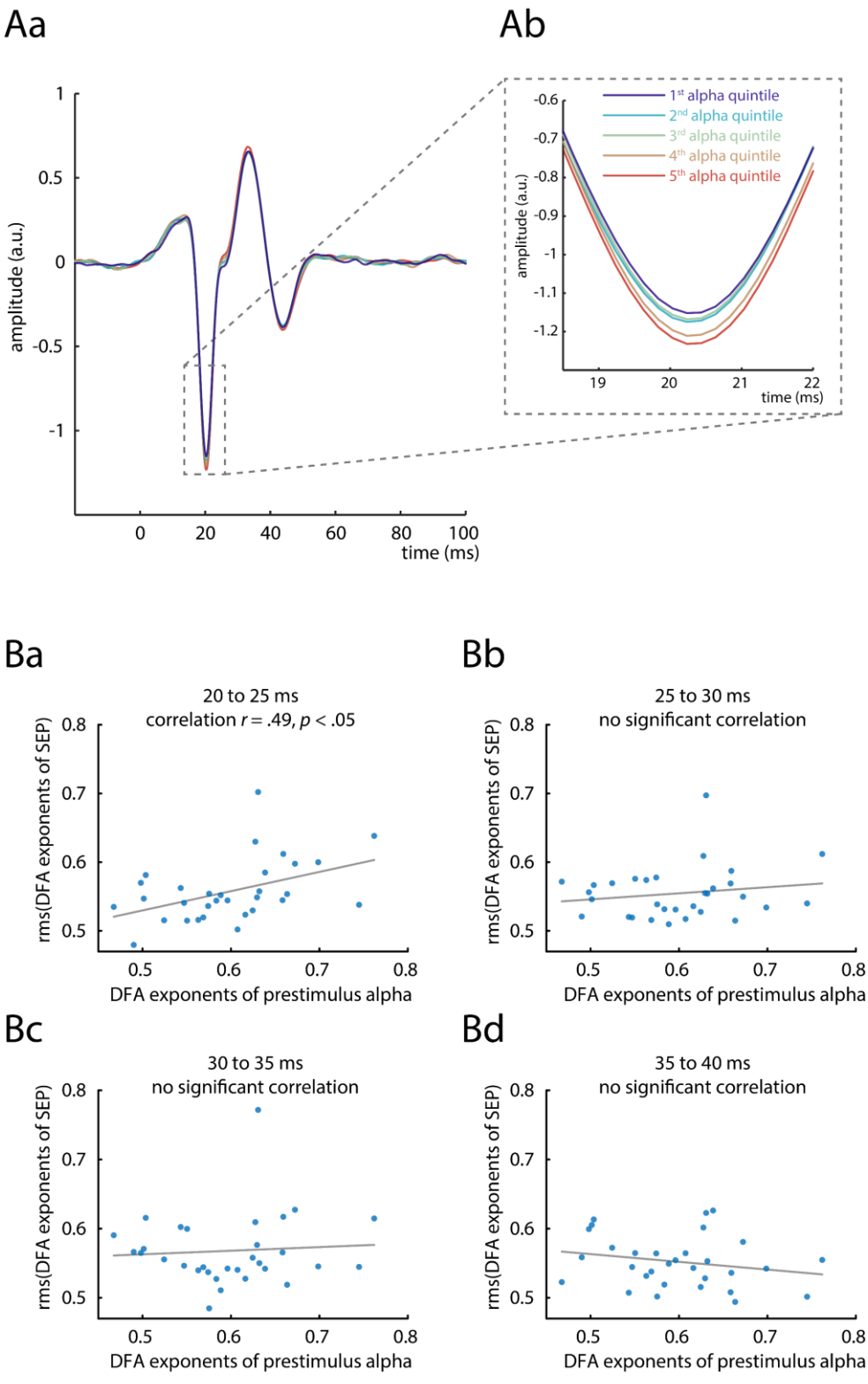

Fig. 9. Relation between pre-stimulus alpha band activity and the early SEP. Panels Aa and Ab depict the SEP plotted by quintiles of pre-stimulus alpha band amplitude, demonstrating their relationship for the N20 component peak (Ab). Panels Ba, Bb, Bc, Bd show the correlations between DFA exponents of pre-stimulus alpha amplitude and DFA exponents of the SEP in time windows from 20 to 25, 25 to 30, 30 to 35, and 35 to 40 ms, respectively. The DFA exponents of the SEP were aggregated over time points using root-mean-square (rms).

3 Discussion

In the present study, we probed instantaneous excitability changes of the somatosensory cortex by applying median nerve stimuli and evaluating single-trial SEP amplitudes in the range of the N20 component which is assumed to reflect excitatory post-synaptic potentials (EPSPs) of the first thalamo-cortical volley (Allison et al., 1991; Bruyns-Haylett et al., 2017; Wikström et al., 1996). Fluctuations of cortical excitability demonstrated power-law dynamics across trials, consistent with the hypothesis that neuronal systems operate close to a critical state (Beggs & Plenz, 2003; Linkenkaer-Hansen et al., 2001; Palva et al., 2013; Poil, Hardstone, Mansvelder, & Linkenkaer-Hansen, 2012; Priesemann et al., 2013). Most likely, these power-law dynamics were of cortical origin as DFA exponents were not increased in peripheral or subcortical neural signals. In addition, fluctuations in alpha band activity and initial cortical excitation were related regarding their amplitudes as well as their temporal structure as measured by DFA. For the first time, these findings thus link critical dynamics in ongoing and evoked activity as measured non-invasively in the human EEG, and directly associate the observed power-law dynamics with variability in cortical excitability.

Neurophysiological basis of temporal fluctuations in the early SEP

The observed power-law dynamics were calculated on the basis of amplitude fluctuations in the early SEP which has previously been shown to reflect EPSPs in the primary somatosensory cortex (Allison et al., 1991; Bruyns-Haylett et al., 2017; Wikström et al., 1996). In principle, the scalp EEG is sensitive to relative changes in collective charge distributions resulting from neuronal activation manifested in primary post-synaptic currents (PSCs; Ilmoniemi & Sarvas, 2019; Kandel, Schwartz, & Jessell, 2000; Lopes da Silva, 2004). Since the scalp EEG aggregates the signal of many neuronal populations, its magnitude also depends on the number of neurons involved. Hence, the magnitude of an EEG potential emerging

through synchronous activity of a well-specified neuron population, as is assumed for the N20 component of the SEP, should follow the general relationship

$$U \sim I * N_{neurons} * LF$$

where *U* denotes the magnitude of the potential on scalp level, *I* the sum of local primary post-synaptic currents, and *LF* the lead field coefficient projecting source activity to the electrodes on the scalp. Since intensity and position of the electrical nerve stimulation was kept constant in our paradigm, we expect an approximately constant number of neurons to have been involved in the generation of SEPs in the primary somatosensory cortex. Also, *LF* is a constant reflecting the conductance of the head tissues and the stable dipole orientation of the N20 component.

Therefore, we believe that primarily the variability of PSCs contributed to the amplitude fluctuations of the early part of the SEP, reflecting instantaneous changes of cortical excitability. This notion is corroborated by findings in basic physiology, where pre-stimulus membrane potential modulations have been found to be associated with variability in subsequent PSPs and PSCs (Deisz, Fortin, & Zieglgansberger, 1991). Specifically, pre-stimulus depolarization facilitates the generation of spiking activity (Azouz & Gray, 1999) and thus represents a state of higher neuronal excitability (Castro-Alamancos, 2009). Hence, temporal dynamics on a cellular level, manifested in collective membrane fluctuations, might lead to excitability changes which determine the magnitude of PSCs and eventually translate to fluctuations of the SEPs across trials, that is, specifically the N20 component of the SEP in our study.

What do temporal dynamics in SEPs tell about the functioning of the neuronal system?

DFA exponents of SEP amplitudes significantly exceeded $\alpha = 0.5$, thus reflecting long-range dependencies of SEPs across trials. That is, the SEP of a given stimulation event is related to the history of previous stimulation events, and also contains information about the SEPs of subsequent stimulation events. In our data, this relationship held for time windows of up to 70 trials, equivalent to around 50 seconds. Furthermore, we used the early part of the SEP as a

probe of excitability of the somatosensory cortex at the moment of stimulation, that is, as a probe of the instantaneous system state of the involved neuron populations in this particular cortical area. Therefore, the observed power-law dynamics suggest that instantaneous system states of the primary somatosensory cortex are characterized by long-range temporal dependencies and do not fluctuate stochastically independently over time.

Both spatial and temporal power-law dynamics in system states have often been interpreted within the hypothesis that the underlying system is poised at a critical state (Bak et al., 1987; P. Bak et al., 1988; Beggs & Plenz, 2003; Sethna et al., 2001). In various models of complex systems, such as the Abelian Sand Pile model (Bak et al., 1987), the Kuramoto model (Kuramoto, 1984), and the Ising model (Ising, 1925), power-law dynamics can be found when they are at the border of a phase transition (Kitzbichler et al., 2009), which has been referred to as the *critical state* (Bak et al., 1987; P. Bak et al., 1988; Beggs & Plenz, 2003). Crucially, it has been shown that information transfer is optimized when a system operates at the critical state (Kinouchi & Copelli, 2006; Shew & Plenz, 2013) making the criticality hypothesis an appealing approach to parsimoniously explain the still poorly understood processing capabilities of the central nervous system.

Conceptually, the temporal dynamics we observed in our data can be seen in analogy to system dynamics observed in above models, as depicted for the Ising model in Figure 2. Usually, long-range dependencies are quantified by certain power-law relationships in these models, such as the distribution of size and duration of neuronal avalanches (Sethna et al., 2001). In the present study, however, we report power-law dynamics in the temporal domain (i.e., SEPs across trials). This finding is in line with previous M/EEG studies reporting long-range temporal correlations (LRTCs) for fluctuations in alpha band activity (Linkenkaer-Hansen et al., 2001; Linkenkaer-Hansen, Nikulin, Palva, Kaila, & Ilmoniemi, 2004; Palva et al., 2013), which could also be replicated in the present study. Importantly, simulations using the Ising model have shown that a system at a critical state, characterized by power-law dynamics in the spatial

domain, indeed expresses power-law dynamics when observing its behavior in the temporal domain, too (Zhao et al., 2017). Thus, the observed long-range *temporal* dependencies in cortical excitability in our data may indicate that the system operates close to a critical state also in the *spatial* domain. Specifically, neuronal excitability may differ across the network of neurons that is involved in the generation of the SEP in the primary somatosensory cortex, which, in turn, would lead to a spread of activation of the SEP in line with scale-free behavior of neuronal avalanches as observed in the seminal paper by Beggs and Plenz (2003) for neuronal dynamics in slices of the rat somatosensory cortex. We now extend this notion by showing that signatures of critical dynamics can also be present in the *human* primary somatosensory cortex. Accordingly, the power-law dynamics we observed in early SEPs may reflect intrinsic properties of the underlying networks which may be built and function in such a way that the activation propagation is similar to that observed at critical states.

In addition, assuming that fluctuations of the early SEP reflect changes in EPSCs which in turn depend on pre-stimulus membrane potentials, it follows that these dynamics may be manifested in ongoing modulations of membrane potentials. Intriguingly, dynamics close to criticality have been demonstrated for membrane potential fluctuations in pyramidal neurons of the visual cortices in turtles (Johnson et al., 2019), consistent with our idea of the origin of power-law dynamics in early human SEPs.

Of course, this notion should be treated with some caution as it is based on the strong assumption that mechanisms observed in single-cell recordings (in animals) can be generalized to cell populations in the human cortex. Nevertheless, the present findings could represent the missing link between power-law dynamics on micro (single-cell) and macro (cell population) scale and would relate findings of criticality in neuronal avalanches to non-invasively measured EEG potentials in humans.

Temporal specificity of the DFA exponent increases

Interestingly, we found two prominent peaks in the DFA exponent time course, one at around 25 ms, and the other at around 33 ms (Fig. 6). Although the first significant DFA exponent cluster started together with the peak of the N20 component, the first DFA exponent peak appeared slightly later. This suggests that long-range temporal dependencies are not primarily pronounced in N20 peak amplitudes but rather reflect the variation of the SEP returning back to baseline. The second DFA time course peak co-occurred with the second prominent peak of the SEP, the P35 component. This second DFA peak most likely reflects activity propagated from the N20 component to the P35 as these two components moderately covaried in our data. Taken together, we conclude that power-law dynamics started to rise around the peak of the N20 component but reached their full extent only a few milliseconds later. This may reflect activity of a more distributed network involved in the SEP after the N20 component, potentially also comprising some mixture of inhibitory processes.

Dissociation of temporal dynamics in the cortex from peripheral and subcortical variability

The fact that DFA exponents were not systematically higher than $\alpha = 0.5$ earlier than the N20 component suggests that the generators of power-law dynamics were located in the primary somatosensory cortex. In addition, we applied the following control analyses to examine the origin of these dynamics in more detail.

First, we inspected the sources of the SEP from which we derived the power-law metrics. In all participants, the single-trial analysis using CCA resulted in one component that showed a tangential spatial pattern (therefore referred to as *tangential CCA component*; left panels in Fig. 4). We chose this component because both the time course and the spatial pattern suggested that the N20-P35 complex of the SEP is well preserved in this CCA component. Indeed, the source reconstruction confirmed that the strongest generators of this component lay in the

anterior wall of the post-central gyrus (Fig. 4E) as is expected from the literature for the N20 component (Allison et al., 1991).

Second, it is conceivable that the power-law dynamics in the early SEP stemmed from fluctuations in peripheral nerve excitation. To control for this, we measured the compound nerve action potential (CNAP) of the median nerve on the inner side of the upper arm. We did not find increased DFA exponents in this measure. Thus, peripheral nerve activity cannot account for the power-law dynamics in the SEP.

Third, sub-cortical structures may play a role in shaping the variability of the cortical response. The thalamus represents the last processing stage before stimulus information enters the cortex. Therefore, investigating variability on this level should inform about whether power-law dynamics were of cortical or sub-cortical nature. The P15 component of the SEP is assumed to reflect thalamic processing of median nerve stimuli (Albe-Fessard et al., 1986). In our data, a CCA component was identified in a subsample of 13 subjects, which showed a peak at 15 ms and a spatial pattern suggesting a deep medial source (Fig. 7C and 7E). Importantly, the variability of this activity presumably originating in the thalamus, did not express power-law dynamics.

Having found no evidence for power-law dynamics arising earlier than cortical processing stages, we conclude that these temporal dynamics most likely are of *cortical* origin.

Underestimation of power-law dynamics due to signal-to-noise ratio

It is known that the signal-to-noise ratio (SNR) has an impact on the estimation of DFA exponents (Blythe et al., 2014), that is, even a signal with an exponent of $\alpha = 1.0$ would result in lower DFA exponents when being contaminated with strong noise characterized by exponents of $\alpha \approx 0.5$. To account for this, we estimated the SNR of the single-trial SEPs and simulated measurement scenarios with varying SNRs and DFA exponents of a signal mixed with white noise. The simulation results indeed indicated that our empirical DFA exponents

underestimated the underlying DFA exponents of the signal. Given our single-trial SNR, the simulation suggested an underlying DFA exponent of $\alpha \approx 0.63$ (Fig. 8), which is in the range of power-law dynamics reported in previous M/EEG studies for alpha band activity (Linkenkaer-Hansen et al., 2001; Palva et al., 2013). However, the estimation of unbiased DFA exponents derived from our simulation is a rather conservative estimate: First, we only assumed one noise source to be mixed with the signal. This is probably not true for the EEG as there will be a vast number of noise sources in reality, thus further degrading the estimation of DFA exponents. Second, the interval in which we estimated the signal (i.e., in the range of the early SEP) is not noise free. Hence, the signal term contained in the SNR is also a mixture of both signal and noise, biasing the SNR towards higher values. Third, the "signal" which is relevant for DFA applied across trials is, strictly speaking, not the amplitude of the single-trial SEP in relation to baseline (as was used for our SNR estimate) but rather the fluctuation of single-trial amplitudes across trials. Thus, the *effective* SNR for DFA was most likely even smaller and, with a DFA exponent of $\alpha \approx 0.63$, the power-law dynamics of the neuronal system are most likely still underestimated.

Relationship between pre-stimulus alpha activity and initial cortex excitation

Since it has been claimed that oscillatory activity in the alpha band reflects cortical excitability (Klimesch et al., 2007; Madsen et al., 2019; Pfurtscheller et al., 1996; Romei et al., 2008; Sauseng, Klimesch, Gerloff, & Hummel, 2009; Zrenner, Desideri, Belardinelli, & Ziemann, 2017), we tested whether this measure was related to the initial cortex excitation as measured by the N20 amplitude. Following a rather simplistic notion that higher excitability leads to larger brain responses, one might assume larger SEP amplitudes in the EEG being present at states of higher cortical excitability. However in our data, lower alpha band activity, typically referred to as state of increased excitability, was associated with smaller (less negative) N20 amplitudes. At first sight, this finding thus seems to contradict the hypothesis of

alpha oscillations representing functional inhibition (Jensen & Mazaheri, 2010; Klimesch et al., 2007). Yet, it may be explained in a straightforward manner by the neurophysiological basis of EEG generation.

As outlined above, EEG cannot directly measure PSPs, but reflects relative changes in collective charge distributions produced by post-synaptic *currents* (PSCs). Now, at states of high excitability (i.e., pre-stimulus membrane depolarization), the electrical driving force for inward currents is decreased and less current is needed to reach the threshold potential for excitatory responses (Castro-Alamancos, 2009). This leads to *decreased* PSCs at high excitability states (Deisz et al., 1991), which would result in lower amplitudes in the EEG signal. Hence, assuming alpha activity to be associated with neuronal excitability, on a cellular level possibly reflected in the membrane potential, one should rather expect *decreased* N20 amplitudes following *low* pre-stimulus alpha activity (higher depolarization). As this relationship held true for our data, we argue that our findings are in fact in line with the alpha inhibition hypothesis and may furthermore shed light on the functional link between ongoing alpha activity and evoked responses which might be manifested in modulations of membrane potentials on a cellular level.

Adding to the relationship between pre-stimulus oscillatory and evoked activity, DFA exponents of pre-stimulus alpha activity and DFA exponents of the early part of the SEP were correlated across subjects. Interestingly, this relation only held for the SEP time range between 20 and 25 ms, which corresponds to the first cluster of increased DFA exponents. This might indicate that DFA exponents of SEPs and alpha oscillations reflect similar underlying brain dynamics, which can be tested both with evoked responses and ongoing oscillations. Although we cannot completely rule out that general data quality (i.e., SNR) influenced the correlation between DFA exponents in alpha band activity and in the SEP across subjects, this alternative explanation seems rather unlikely at this point since the SNRs of the SEP and DFA exponents of alpha activity were not found to be correlated in our data.

Taken together, the two measures of cortical excitability, alpha band activity and early SEP amplitudes, indeed seem to closely correspond regarding both their amplitudes and temporal structure, suggesting similar organizing principles. Yet, the current data cannot disentangle whether there is a causal relationship between pre-stimulus alpha band and early SEP fluctuations, as it cannot be excluded that a common factor, reflected in the underlying system state, gives rise to these phenomena independently from each other.

Implications for the perspective on neural variability

Why neuronal systems express a large variability, particularly in perceptual processes, has been an enduring question for many years. Previous studies investigated variability in terms of its strength (Churchland et al., 2010; Dinstein et al., 2015; Garrett et al., 2013) and regarding its accompanying neuronal signatures (Arieli et al., 1996; Iemi et al., 2019; Romei, Gross, & Thut, 2010; Sadaghiani et al., 2010; Vanrullen et al., 2011). In the present study, we approached neural variability, specifically of cortical excitability, from a different perspective and examined its temporal dynamics. In particular, it may be that not only the strength of variability but rather its specific temporal signature is important for a proper functioning of the underlying system. We believe that such temporal dynamics might be of a very special type, i.e., those corresponding to a critical state, which is manifested in the presence of long-range temporal dependencies. This type of variability has been shown to be associated with the maximization of the dynamic range, as well as optimized information processing and capacity (Kinouchi & Copelli, 2006; Shew & Plenz, 2013). Hence, this notion represents a compelling account for why neuronal variability can be functionally needed and how this variability is actually embedded in the complex dynamics of the human neuronal system.

Conclusions

Cortical excitability, as probed by early SEPs and pre-stimulus alpha band activity, demonstrated power-law dynamics over time, indicating long-range temporal dependencies of

instantaneous brain states. Thus, excitability changes do not seem to occur stochastically independently (i.e., like white noise) but do possess a temporal structure. Furthermore, this observation may shed light on the spatio-temporal organization of the underlying neuronal system, as power-law dynamics are traditionally seen as a key signature of a complex system poised at a transition state between stability und instability, the so-called critical state. Although such temporal dynamics are not a direct proof for the presence of criticality, we consider our present findings of power-law dynamics in early SEP amplitudes as another complementary evidence consistent with the hypothesis that the neuronal system indeed operates in proximity to a critical state.

4 Methods

Participants

EEG data were recorded from 33 male, human subjects. Two subjects had to be excluded because no clear SEPs were visible in the single-trial analysis, probably due to suboptimal placement of the stimulation electrodes and a low SNR of the EEG. The remaining sample of 31 subjects had an average age of M = 26.9 years (SD = 5.0). All participants were right-handed (lateralization score, M = +92.9, SD = 11.7), as assessed with the Edinburgh Handedness Inventory (Oldfield, 1971), and did not report any neurological or psychiatric disease. All participants gave informed consent and the study was approved by the local ethics committee.

Stimuli

Somatosensory stimuli were applied using electrical stimulation of the median nerve. A non-invasive bipolar stimulation electrode was positioned at the left wrist (cathode proximal). The electrical stimuli were designed as squared pulses of a duration of 200 µs. The stimulus

intensity was set to 1.2 x motor threshold leading to clearly visible thumb twitches for every stimulus, as individually determined by a staircase procedure prior to the experiment. Stimuli were applied using a DS-7 constant-current stimulator (Digitimer, United Kingdom).

Procedure

During the experiment, participants were sitting comfortably in a chair their hands extended in front of them on a pillow with their hands in supinated position. Electrical stimuli were presented in a continuous sequence with inter-stimulus intervals (ISI) ranging from 663 to 763 ms (randomly drawn from a uniform distribution; $ISI_{average}$ = 713 ms). In total, 1000 stimuli were applied divided into two blocks of 500 stimuli each. After the first block, the sequence was interrupted by a short break. Participants were instructed to relax and to fixate with their eyes on a cross on a computer screen in front of them while receiving the stimuli.

Data Acquisition

EEG data were recorded from 60 Ag/AgCl electrodes at a sampling rate of 5000 Hz using an 80 channel EEG system (NeurOne, Bittium, Oulu, Finland) with a bandwidth of 0.16 to 1250 Hz. Electrodes were mounted in an elastic cap (EasyCap, Herrsching, Germany) at the international 10-10 system positions FP1, FPz, FP2, AF7, AF3, AFz, AF4, AF8, F7, F5, F3, F1, Fz, F2, F4, F6, F8, FT9, FT7, FT8, FT10, FC5, FC3, FC1, FC2, FC4, FC6, C5, C3, C1, Cz, C2, C4, C6, CP5, CP3, CP1, CPz, CP2, CP4, CP6, T7, T8, TP7, TP8, P7, P5, P3, P1, Pz, P2, P4, P6, P8, PO7, PO3, PO4, PO8, O1, O2. Four additional electrodes were placed at the outer canthus and at the infraorbital ridge of each eye to record the electro-oculogram (EOG). During recording, the EEG signal was referenced to FCz, POz served as ground. All impedances were kept below 10 kΩ. For source reconstruction, EEG electrode positions were measured in 3D space individually for every subject using Polhemus Patriot (Polhemus, Colchester, Vermont). Additionally, the compound nerve action potential (CNAP) of the median nerve was measured using two bipolar electrodes, positioned at the inner side of the left upper arm.

Structural MRI scans (MPRAGE) of every participant were obtained at a different testing date prior to the experiment on a 3T Siemens Verio, Siemens Skyra or Siemens Prisma scanner (Siemens, Erlangen, Germany).

EEG pre-processing

Stimulation artifacts were cut out and interpolated between -2 to 4 ms relative to stimulus onset using Piecewise Cubic Hermite Interpolating Polynomials (PCHIP). The EEG data were band-pass filtered between 30 and 200 Hz, sliding a 4th order Butterworth filter forwards and backwards over the data to prevent phase shift. With this filter, we specifically focussed on the N20-P35 complex of the SEP. Furthermore, this filter effectively served as baseline correction of the SEP since it removed slow trends in the data, reaching an attenuation of 30 dB at 14 Hz, thus ensuring that fluctuations in the SEP did not arise from fluctuations with slower frequencies (e.g., alpha band activity). (The relationship between decibels (dB) and magnitude is defined as $dB = 20 * log_{10}(magnitude)$.) Bad segments of the data were removed by visual inspection, resulting in 989 trials on average per participant. The data were then re-referenced to an average reference. Eye artefacts were removed using Independent Component Analysis (ICA). For the analysis of SEPs, the data were segmented into epochs from -100 to 600 ms relative to stimulus onset. EEG pre-processing was performed using EEGLAB (Delorme & Makeig, 2004), and custom-written scripts in MATLAB (The MathWorks Inc., Natick, Massachusetts).

Single-trial extraction using CCA

Single-trial SEPs were extracted applying a variant of Canonical Correlation Analysis (CCA), as previously proposed by Waterstraat et al. (2015). CCA is used for finding weights w_x and w_y that mutually maximize the correlation between two signals X and Y, so that:

$$X * w_x \overset{\max corr}{\longleftrightarrow} Y * w_y$$

For extracting single-trial SEPs, we constructed X as a two-dimensional matrix (time by channel) containing all single-trial epochs (concatenated in the time domain) whereas Y contained the average SEP, concatenated as many times as there were epochs (also concatenated in the time domain). The resulting weight matrix w_x represents spatial filters which maximize, in combination with w_y, the correlation between single-trial activity (X) and the average SEP (Y). To particularly focus on the early portion of the SEP, the spatial filters w_x were trained using shorter segments from 5 to 80 ms post-stimulus but applied to the whole epochs from -100 to 600 ms. Applying the spatial filters to the single-trial matrix, we derived a number of spatially distinct components, here denoted as *CCA components*:

$$X_{CCA} = X * w_x \, .$$

To characterize the CCA components in more detail, their spatial patterns were computed as

$$A_{CCA} = cov(X) * w_x \, ,$$

and components were visually identified that showed a tangential spatial pattern over the central sulcus as is typical for the N20-P35 complex (referred to as *tangential CCA components*). Furthermore, components were identified that were characterized by a radial pattern over the central sulcus (referred to as *radial CCA components*), as well as components that showed a peak in the activity time course at 15 ms (referred to as *thalamic CCA components*; only in a subset of the sample). This procedure was performed individually for every subject for the first four CCA components, as sorted by their canonical correlation coefficients. Since CCA is insensitive to the polarity of the signal, the resulting tangential CCA components were standardized so that the N20 always appeared as a negative peak in the SEP (i.e., by inverting their spatial filters w_x, if necessary). Furthermore, CCA is insensitive to the order of trials. Thus, the same spatial filters w_x are obtained when permuting the order of single-trial SEPs and it is therefore not possible that CCA influences the temporal structure of SEP amplitudes across trials.

SEP peak amplitudes and pre-stimulus oscillatory activity

N20 peak amplitudes were defined as the minimum value in single-trial SEPs of the tangential CCA components ±2 ms around the latency of the N20 in the within-subject average SEP. Accordingly, P35 peak amplitudes were extracted.

Pre-stimulus alpha band activity was obtained from data segments between -200 to -10 ms relative to stimulus onset, band-pass filtered between 8 and 13 Hz (8^{th} order Butterworth filter), after mirroring the pre-stimulus segments to both sides in order to reduce filter-related edge effects. To make a direct comparison with the SEP possible, we applied the spatial filter corresponding to the tangential CCA component to the pre-stimulus data. Subsequently, the pre-stimulus alpha envelope was measured by taking the absolute values of the signals processed with the Hilbert transform. To derive one pre-stimulus alpha metric for every trial, amplitudes of the alpha envelope were averaged across the whole pre-stimulus time window.

EEG source reconstruction

To reconstruct the sources of the EEG signal, we estimated leadfield matrices based on individual brain anatomies and individually measured electrode positions. The structural brain scans (MPRAGE) were segmented using the Freesurfer software (http://surfer.nmr.mgh.harvard.edu/), and a 3-shell boundary element model (BEM) was constructed which was used to compute the lead field matrix with OpenMEEG (Gramfort, Papadopoulo, Olivi, & Clerc, 2010; Kybic et al., 2005). For two subjects, a template brain anatomy (ICBM152; Fonov, Evans, McKinstry, Almli, & Collins, 2009) was used as no individual structural MRI scans were available. For one subject, standard electrode positions were used instead of individually measured positions. The leadfield matrices were inverted using eLORETA (Pascual-Marqui, 2007), and sources were reconstructed for the spatial patterns of the tangential and radial CCA components, respectively, for every subject. Next,

individual source spaces were transformed into a common source space based on the ICBM152 template using the spherical co-registration with the FSAverage atlas (Fischl, Sereno, Tootell, & Dale, 1999) derived from Freesurfer, in order to average the obtained sources of the CCA components across subjects. The calculation of the individual head models and visualization of the sources was performed using Brainstorm (Tadel, Baillet, Mosher, Pantazis, & Leahy, 2011). The MATLAB implementation of the eLORETA algorithm is available in the MEG/EEG Toolbox of Hamburg (METH).

Processing of peripheral electrophysiological data (median nerve CNAP)

Stimulation artefacts were cut out and interpolated between -2 to 4 ms relative to stimulus-onset using Piecewise Cubic Hermite Interpolating Polynomials (PCHIP). The peripheral electrophysiological data were high-pass filtered at 70 Hz, sliding a 4th order Butterworth filter forwards and backwards over the data to prevent phase shift. Additionally, notch filters (4th order Butterworth) were applied from 48 to 52 Hz and 148 to 152 Hz, respectively. Analogously to the EEG data, epochs were extracted from -100 to 600 ms relative to stimulus onset.

Detrended Fluctuation Analysis (DFA)

Power-law dynamics in the fluctuations of early SEPs as well as of pre-stimulus alpha band activity were quantified applying Detrended Fluctuation Analysis (DFA; Hardstone et al., 2012; Kantelhardt et al., 2001). DFA calculates the fluctuation (i.e., standard deviation) of a cumulative signal on different time scales and tests whether its distribution follows a power-law: $F(\tau) \sim \tau^{\alpha}$, where F denotes the fluctuation function, τ the signal length (or window size), and α the power-law exponent. The DFA exponent α quantifies the extent of power-law dynamics of a signal, with $\alpha > 0.5$ indicating persistent auto-correlations; whereas $\alpha = 0.5$ is expected for a signal without a correlated temporal structure (i.e., white noise). We analyzed power-law dynamics in the fluctuation of SEP and pre-stimulus alpha amplitudes across trials

in windows ranging from 7 to 70 trials, which correspond to time windows of around 5 to around 50 seconds. The same time windows were selected for the DFA of continuous, ongoing alpha band activity.

Evaluation of SNR

The signal-to-noise ratio of the single-trial SEP, as measured by the tangential CCA component, was quantified as the quotient of the root-mean-square signal in the time range of the SEP (10 to 50 ms) and a pre-stimulus baseline (-50 to -10 ms), so that $SNR = \frac{rms(signal)}{rms(noise)}$.

The same procedure was applied to estimate the SNR of the CNAP and of the thalamic CCA component. For the CNAP we chose time windows from 5 to 8 ms and -8 to -5 ms, and for thalamic activity 12 to 18 ms and -18 to -12 ms, to estimate signal and noise, respectively.

Simulation of the relationship between SNR and DFA exponent

Signals with DFA exponents systematically varying in the range from $\alpha = 0.5$ to $\alpha = 0.8$ were generated by filtering white noise with IIR filters whose coefficients depended on the desired DFA exponents as described in Schaworonkow et al. (2015) according to the algorithm of Kasdin (1995). The length of these time series was set to 1000 data points corresponding to our empirical data from the SEP fluctuation across trials. These time series were mixed with white noise, that is, stochastically independent time series with DFA exponents of $\alpha = 0.5$, being consistent with DFA exponents measured before stimulus-onset in our empirical data. The time series with varying DFA exponents were mixed with the noise at varying SNRs ranging from 0.001 to 6, defined as $SNR = \frac{rms(signal)}{rms(noise)}$. This procedure was repeated 100 times to account for the variance in the generation of random time series. Subsequently, DFA exponents of the mixed time series were measured and the average DFA exponent of the simulated signal was identified for which the SNR and DFA exponent of the mixed time series corresponded to our

empirical analysis of SEP fluctuations. For visualization purposes, the results of the simulation are displayed in Figure 8 only for a sub-range of DFA exponents and SNRs.

Simulation of the influence of temporal filtering on DFA exponents

To confirm that our temporal filtering did not cause the DFA exponent increases in the early SEP, we applied the same filtering to surrogate data with stochastically independent SEP fluctuations. SEP fluctuations across trials were simulated by decreasing or increasing an average SEP time course by a randomly generated factor for every trial. These signals were superimposed on continuous pink noise which was band-pass filtered between 30 and 200 Hz (4^{th} order Butterworth filter), using a signal-to-noise ratio of 2, a typical value for empirical data. Subsequently, DFA was applied across trials for every time sample of the simulated SEP, corresponding to above described DFA analyses of the empirical SEPs.

Statistical analyses

We compared the empirical DFA exponent time courses to surrogate data and applied cluster-based permutation tests to assess whether, and at which latencies, DFA exponents were significantly higher than it would be expected for stochastically independent fluctuation (i.e., white noise). First, we determined the expected DFA exponents for stochastically independent fluctuation by shuffling the trial order of our data and applying DFA to it. To account for variability due to random shuffling, this step was repeated 1000 times, and DFA exponents of these iterations were averaged, yielding an average surrogate DFA exponent time course for every subject. (Averaged across all samples and subjects, the mean DFA exponent was $\alpha = .512$, thus slightly increased as compared to the theoretical DFA exponent of white noise of $\alpha = .5$. This small empirical deviation may have been caused by the asymptotic behaviour of DFA for small window sizes.) Next, the DFA exponents of the data with intact trial order were compared to the average DFA exponents of the surrogate data, using a two-sample t-test, resulting in a *t* value for every comparison over the time course of the SEP. To obtain clusters of increased

DFA exponents, *t* values were thresholded at p_{pre} = .001. Within clusters, *t* values were summed up to cluster *t* values $t_{cluster,empirical}$. The same procedure was repeated 1000 times for the surrogate data, always comparing one surrogate dataset to the average surrogate data, which provided us with the distribution of cluster *t* values under the null hypothesis. Next, a cut-off value $t_{cluster,crit}$ was defined at the 99.9th percentile corresponding to a cluster threshold of $p_{cluster}$ = .001. Finally, $t_{cluster,empirical}$ of all clusters in the empirical DFA exponent time course were compared to $t_{cluster,crit}$ to identify clusters of significantly increased DFA exponents. With this procedure, we controlled for the number of samples over the SEP time course, inter-subject variability, and the distribution of amplitude values of the SEP from which DFA exponents were derived.

Analogously, DFA exponents of pre-stimulus alpha band activity were statistically tested using a t-test on group-level to compare them to the average DFA exponents of the null distribution, which was calculated from 1000 surrogate datasets with shuffled trial order. Similarly, the statistical significance of the DFA exponents of continuous alpha band activity was tested, however shuffling samples instead of trials to obtain DFA exponents under the null hypothesis.

To test the relationship of SNR and DFA exponents, we correlated the average SNR of single-trial SEPs with the area-under-the-curve (AUC) of DFA exponents between 10 and 50 ms post-stimulus, across participants using Spearman correlation.

Furthermore, we assessed the relationship between single-trial N20 peak amplitudes and pre-stimulus alpha amplitudes using a linear-mixed-effects model with *subject* as random factor, estimating the fixed effect as well as the random slope of the predictor *pre-stimulus alpha amplitude* with the dependent variable *N20 peak amplitude* (intercepts were included both for the fixed and random effects). Denominator degrees of freedom were adjusted using Satterthwaite´s method (Satterthwaite, 1946) to derive a *p* value for the fixed effect of *pre-stimulus alpha amplitude* as implemented in the R package lmerTest (Kuznetsova, Brockhoff,

& Christensen, 2017). Additionally, the relationship between N20 peak amplitudes and pre-stimulus alpha amplitudes was assessed with a permutation-based approach in which we compared their Spearman correlation coefficients with those from surrogate pre-stimulus alpha amplitudes with the same auto-correlated structure but shuffled phases generated by Adjusted Amplitude Fourier Transform (Theiler, Eubank, Longtin, Galdrikian, & Doyne Farmer, 1992), as suggested in Schaworonkow et al. (2015). Empirical correlation coefficients were averaged across subjects after Fisher´s Z transformation and compared with the null distribution of 10000 averaged correlation coefficients from the surrogate analyses to obtain the corresponding *p* value.

Also, we correlated DFA exponents of pre-stimulus alpha activity and DFA exponents of the SEP. To account for the variability in the DFA exponent time course in the early SEP, we calculated the root-mean-square of DFA exponents in four subsequent time windows, 20 to 25, 25 to 30, 30 to 35, and 35 to 40 ms, and computed their Spearman correlation coefficients with the DFA exponents of pre-stimulus alpha activity, respectively. To control for the resulting multiple testing, we applied Bonferroni correction.

Finally, the relation between single-trial N20 and P35 peak amplitudes was tested using a linear-mixed-effects model with the dependent variable P35 peak amplitude, estimating the fixed effect and the random slope of the independent variable N20 peak amplitude including subject as random factor (intercepts were included both for the fixed and random effects). Again, Satterthwaite´s method (Satterthwaite, 1946) was used to derive a p value for the fixed effect.

For all correlation analyses the significance level was set to $p = .05$. Correlation analyses as well as permutation-based statistics were performed in MATLAB (version 2017b, The MathWorks Inc., Natick, Massachusetts). The linear-mixed-effects models were calculated in R (version 3.5.1, R Core Team, 2018) using the lme4 (Bates, Mächler, Bolker, & Walker, 2015) and lmerTest packages (Kuznetsova et al., 2017).

Acknowledgements

We thank Sylvia Stasch for participant recruitment and help during data collection, as well as Alice Hodapp for supporting the source reconstruction of the EEG.

References

Albe-Fessard, D., Tasker, R., Yamashiro, K., Chodakiewitz, J., & Dostrovsky, J. (1986). Comparison in man of short latency averaged evoked potentials recorded in thalamic and scalp hand zones of representation. *Electroencephalography and Clinical Neurophysiology/Evoked Potentials Section*, *65*(6), 405–415. https://doi.org/10.1016/0168-5597(86)90020-1

Allison, T., McCarthy, G., Wood, C. C., & Jones, S. J. (1991). Potentials Evoked in Human and Monkey Cerebral Cortex by Stimulation of the Median Nerve. *Brain*, *114*(6), 2465–2503. https://doi.org/10.1093/brain/114.6.2465

Arieli, A., Sterkin, A., Grinvald, A., & Aertsen, A. (1996). Dynamics of ongoing activity: Explanation of the large variability in evoked cortical responses. *Science*, *273*(5283), 1868–1871.

Arviv, O., Goldstein, A., & Shriki, O. (2015). Near-Critical Dynamics in Stimulus-Evoked Activity of the Human Brain and Its Relation to Spontaneous Resting-State Activity. *The Journal of Neuroscience*, *35*(41), 13927–13942. https://doi.org/10.1523/JNEUROSCI.0477-15.2015

Azouz, R., & Gray, C. M. (1999). Cellular Mechanisms Contributing to Response Variability of Cortical Neurons In Vivo. *The Journal of Neuroscience*, *19*(6), 2209–2223. https://doi.org/10.1523/JNEUROSCI.19-06-02209.1999

Bak, Tang, & Wiesenfeld (1987). Self-organized criticality: An explanation of the 1/f noise. *Physical Review Letters*, *59*(4), 381–384. https://doi.org/10.1103/PhysRevLett.59.381

Bak, P., Tang, C., & Wiesenfeld, K. (1988). Self-organized criticality. *Physical Review A*, *38*(1), 364–374. https://doi.org/10.1103/PhysRevA.38.364

Bates, D., Mächler, M., Bolker, B., & Walker, S. (2015). Fitting Linear Mixed-Effects Models Using lme4. *Journal of Statistical Software*, *67*(1). https://doi.org/10.18637/jss.v067.i01

Becker, R., Reinacher, M., Freyer, F., Villringer, A., & Ritter, P. (2011). How ongoing neuronal oscillations account for evoked fMRI variability. *The Journal of Neuroscience*, *31*(30), 11016–11027. https://doi.org/10.1523/JNEUROSCI.0210-11.2011

Beggs, J. M., & Plenz, D. (2003). Neuronal Avalanches in Neocortical Circuits. *The Journal of Neuroscience*, *23*(35), 11167–11177. https://doi.org/10.1523/JNEUROSCI.23-35-11167.2003

Blythe, D. A. J., Haufe, S., Müller, K.‐R., & Nikulin, V. V. (2014). The effect of linear mixing in the EEG on Hurst exponent estimation. *NeuroImage*, *99*, 377–387. https://doi.org/10.1016/j.neuroimage.2014.05.041

Botcharova, M., Farmer, S. F., & Berthouze, L. (2014). Markers of criticality in phase synchronization. *Frontiers in Systems Neuroscience*, *8*, 176. https://doi.org/10.3389/fnsys.2014.00176

Britten, K. H., Newsome, W. T., Shadlen, M. N., Celebrini, S., & Movshon, J. A. (1996). A relationship between behavioral choice and the visual responses of neurons in macaque MT. *Visual Neuroscience*, *13*(01), 87–100. https://doi.org/10.1017/S095252380000715X

Bruyns-Haylett, M., Luo, J., Kennerley, A. J., Harris, S., Boorman, L., Milne, E., . . . Zheng, Y. (2017). The neurogenesis of P1 and N1: A concurrent EEG/LFP study. *NeuroImage*, *146*, 575–588. https://doi.org/10.1016/j.neuroimage.2016.09.034

Castro-Alamancos, M. A. (2009). Cortical up and activated states: Implications for sensory information processing. *The Neuroscientist*, *15*(6), 625–634. https://doi.org/10.1177/1073858409333074

Churchland, M. M., Yu, B. M., Cunningham, J. P., Sugrue, L. P., Cohen, M. R., Corrado, G. S., . . . Shenoy, K. V. (2010). Stimulus onset quenches neural variability: A widespread cortical phenomenon. *Nature Neuroscience*, *13*(3), 369–378. https://doi.org/10.1038/nn.2501

Deisz, R. A., Fortin, G., & Zieglgansberger, W. (1991). Voltage dependence of excitatory postsynaptic potentials of rat neocortical neurons. *Journal of Neurophysiology*, *65*(2), 371–382. https://doi.org/10.1152/jn.1991.65.2.371

Delorme, A., & Makeig, S. (2004). Eeglab: An open source toolbox for analysis of single-trial EEG dynamics including independent component analysis. *Journal of Neuroscience Methods*, *134*(1), 9–21. https://doi.org/10.1016/j.jneumeth.2003.10.009

Dinstein, I., Heeger, D. J., & Behrmann, M. (2015). Neural variability: Friend or foe? *Trends in Cognitive Sciences*, *19*(6), 322–328. https://doi.org/10.1016/j.tics.2015.04.005

Fedele, T., Scheer, H.‐J., Burghoff, M., Waterstraat, G., Nikulin, V. V., & Curio, G. (2013). Distinction between added-energy and phase-resetting mechanisms in non-invasively detected somatosensory evoked responses. *Conference Proceedings: IEEE Engineering in Medicine and Biology Society. Annual Conference*, *2013*, 1688–1691. https://doi.org/10.1109/EMBC.2013.6609843

Fischl, B., Sereno, M. I., Tootell, R. B.H., & Dale, A. M. (1999). High-resolution intersubject averaging and a coordinate system for the cortical surface. *Human Brain Mapping*, *8*(4), 272–284. https://doi.org/10.1002/(SICI)1097-0193(1999)8:4<272::AID-HBM10>3.0.CO;2-4

Fonov, V. S., Evans, A. C., McKinstry, R. C., Almli, C. R., & Collins, D. L. (2009). Unbiased nonlinear average age-appropriate brain templates from birth to adulthood. *NeuroImage*, *47*, S102. https://doi.org/10.1016/S1053-8119(09)70884-5

Forschack, N., Nierhaus, T., Müller, M. M., & Villringer, A. (2017). Alpha-Band Brain Oscillations Shape the Processing of Perceptible as well as Imperceptible Somatosensory Stimuli during Selective Attention. *The Journal of Neuroscience*, *37*(29), 6983–6994. https://doi.org/10.1523/JNEUROSCI.2582-16.2017

Fox, M. D., & Raichle, M. E. (2007). Spontaneous fluctuations in brain activity observed with functional magnetic resonance imaging. *Nature Reviews. Neuroscience*, *8*(9), 700–711. https://doi.org/10.1038/nrn2201

Friedman, N., Ito, S., Brinkman, B. A. W., Shimono, M., DeVille, R. E. L., Dahmen, K. A., . . . Butler, T. C. (2012). Universal critical dynamics in high resolution neuronal avalanche data. *Physical Review Letters*, *108*(20), 208102. https://doi.org/10.1103/PhysRevLett.108.208102

Garrett, D. D., Samanez-Larkin, G. R., MacDonald, S. W. S., Lindenberger, U., McIntosh, A. R., & Grady, C. L. (2013). Moment-to-moment brain signal variability: A next frontier in human brain mapping? *Neuroscience and Biobehavioral Reviews*, *37*(4), 610–624. https://doi.org/10.1016/j.neubiorev.2013.02.015.

Gramfort, A., Papadopoulo, T., Olivi, E., & Clerc, M. (2010). Openmeeg: Opensource software for quasistatic bioelectromagnetics. *Biomedical Engineering Online*, *9*, 45. https://doi.org/10.1186/1475-925X-9-45

Grill-Spector, K., Henson, R. N. A., & Martin, A. (2006). Repetition and the brain: Neural models of stimulus-specific effects. *Trends in Cognitive Sciences*, *10*(1), 14–23. https://doi.org/10.1016/j.tics.2005.11.006

Hahn, G., Petermann, T., Havenith, M. N., Yu, S., Singer, W., Plenz, D., & Nikolic, D. (2010). Neuronal avalanches in spontaneous activity in vivo. *Journal of Neurophysiology*, *104*(6), 3312–3322. https://doi.org/10.1152/jn.00953.2009

Hardstone, R., Poil, S.-S., Schiavone, G., Jansen, R., Nikulin, V. V., Mansvelder, H. D., & Linkenkaer-Hansen, K. (2012). Detrended fluctuation analysis: A scale-free view on neuronal oscillations. *Frontiers in Physiology*, *3*, 450. https://doi.org/10.3389/fphys.2012.00450

Iemi, L., Busch, N. A., Laudini, A., Haegens, S., Samaha, J., Villringer, A., & Nikulin, V. V. (2019). Multiple mechanisms link prestimulus neural oscillations to sensory responses. *ELife*, *8*. https://doi.org/10.7554/eLife.43620

Ilmoniemi, R. J., & Sarvas, J. (2019). *Brain Signals: Physics and Mathematics of MEG and EEG*. *neuroscience*.

Ising, E. (1925). Beitrag zur Theorie des Ferromagnetismus. *Zeitschrift für Physik*, *31*(1), 253–258. https://doi.org/10.1007/BF02980577

Jansen, B. H., & Brandt, M. E. (1991). The effect of the phase of prestimulus alpha activity on the averaged visual evoked response. *Electroencephalography and Clinical Neurophysiology*, *80*(4), 241–250.

Jensen, O., & Mazaheri, A. (2010). Shaping functional architecture by oscillatory alpha activity: Gating by inhibition. *Frontiers in Human Neuroscience*, *4*, 186. https://doi.org/10.3389/fnhum.2010.00186

Johnson, J. K., Wright, N. C., Xia, J., & Wessel, R. (2019). Single-cell membrane potential fluctuations evince network scale-freeness and quasicriticality. *The Journal of Neuroscience*, 3163-18. https://doi.org/10.1523/JNEUROSCI.3163-18.2019

Kandel, E. R., Schwartz, J. H., & Jessell, T. M. (Eds.). (2000). *Principles of neural science* (4. ed.). New York, NY: McGraw-Hill Health Professions Division.

Kantelhardt, J. W., Koscielny-Bunde, E., Rego, H. H.A., Havlin, S., & Bunde, A. (2001). Detecting long-range correlations with detrended fluctuation analysis. *Physica A: Statistical Mechanics and its Applications*, *295*(3-4), 441–454. https://doi.org/10.1016/S0378-4371(01)00144-3

Kasdin, N. J. (1995). Discrete simulation of colored noise and stochastic processes and 1/f/sup α/ power law noise generation. *Proceedings of the IEEE*, *83*(5), 802–827. https://doi.org/10.1109/5.381848

Kinouchi, O., & Copelli, M. (2006). Optimal dynamical range of excitable networks at criticality. *Nature Physics*, *2*, 348 EP -. https://doi.org/10.1038/nphys289

Kitzbichler, M. G., Smith, M. L. [Marie], Christensen, S. R., & Bullmore, E. (2009). Broadband criticality of human brain network synchronization. *PLoS Computational Biology*, *5*(3), e1000314. https://doi.org/10.1371/journal.pcbi.1000314

Klimesch, W., Sauseng, P., & Hanslmayr, S. (2007). Eeg alpha oscillations: The inhibition-timing hypothesis. *Brain Research Reviews*, *53*(1), 63–88. https://doi.org/10.1016/j.brainresrev.2006.06.003

Kuramoto, Y. (1984). *Chemical Oscillations, Waves, and Turbulence*. Mineola, NY: Dover Publications.

Kuznetsova, A., Brockhoff, P. B., & Christensen, R. H. B. (2017). lmerTest Package: Tests in Linear Mixed Effects Models. *Journal of Statistical Software*, *82*(13). https://doi.org/10.18637/jss.v082.i13

Kybic, J., Clerc, M., Abboud, T., Faugeras, O., Keriven, R., & Papadopoulo, T. (2005). A common formalism for the Integral formulations of the forward EEG problem. *IEEE Transactions on Medical Imaging*, *24*(1), 12–28. https://doi.org/10.1109/TMI.2004.837363

Linkenkaer-Hansen, K., Nikouline, V. V., Palva, J. M., & Ilmoniemi, R. J. (2001). Long-Range Temporal Correlations and Scaling Behavior in Human Brain Oscillations. *The*

Journal of Neuroscience, *21*(4), 1370–1377. https://doi.org/10.1523/JNEUROSCI.21-04-01370.2001

Linkenkaer-Hansen, K., Nikulin, V. V., Palva, J. M., Kaila, K., & Ilmoniemi, R. J. (2004). Stimulus-induced change in long-range temporal correlations and scaling behaviour of sensorimotor oscillations. *European Journal of Neuroscience*, *19*(1), 203–218. https://doi.org/10.1111/j.1460-9568.2004.03116.x

Lopes da Silva, F. (2004). Functional localization of brain sources using EEG and/or MEG data: Volume conductor and source models. *Magnetic Resonance Imaging*, *22*(10), 1533–1538. https://doi.org/10.1016/j.mri.2004.10.010

Madsen, K. H., Karabanov, A. N., Krohne, L. G., Safeldt, M. G., Tomasevic, L., & Siebner, H. R. (2019). No trace of phase: Corticomotor excitability is not tuned by phase of pericentral mu-rhythm. *Brain Stimulation.* Advance online publication. https://doi.org/10.1016/j.brs.2019.05.005

Mathewson, K. E., Lleras, A., Beck, D. M., Fabiani, M., Ro, T., & Gratton, G. (2011). Pulsed out of awareness: Eeg alpha oscillations represent a pulsed-inhibition of ongoing cortical processing. *Frontiers in Psychology*, *2*, 99. https://doi.org/10.3389/fpsyg.2011.00099

Muñoz, M. A. (2018). Colloquium: Criticality and dynamical scaling in living systems. *Reviews of Modern Physics*, *90*(3), 551. https://doi.org/10.1103/RevModPhys.90.031001

Nicholson Peterson, N., Schroeder, C. E., & Arezzo, J. C. (1995). Neural generators of early cortical somatosensory evoked potentials in the awake monkey. *Electroencephalography and Clinical Neurophysiology/Evoked Potentials Section*, *96*(3), 248–260. https://doi.org/10.1016/0168-5597(95)00006-E

Oldfield, R. C. (1971). The assessment and analysis of handedness: The Edinburgh inventory. *Neuropsychologia*, *9*(1), 97–113. https://doi.org/10.1016/0028-3932(71)90067-4

Palva, J. M., Zhigalov, A., Hirvonen, J., Korhonen, O., Linkenkaer-Hansen, K., & Palva, S. (2013). Neuronal long-range temporal correlations and avalanche dynamics are correlated

with behavioral scaling laws. *Proceedings of the National Academy of Sciences of the United States of America*, *110*(9), 3585–3590. https://doi.org/10.1073/pnas.1216855110

Pascual-Marqui, R. D. (2007). Discrete, 3D distributed linear imaging methods of electric neuronal activity. Part 1: exact, zero error localization. *arXiv*. Retrieved from http://arxiv.org/pdf/0710.3341

Petermann, T., Thiagarajan, T. C., Lebedev, M. A., Nicolelis, M. A. L., Chialvo, D. R., & Plenz, D. (2009). Spontaneous cortical activity in awake monkeys composed of neuronal avalanches. *Proceedings of the National Academy of Sciences of the United States of America*, *106*(37), 15921–15926. https://doi.org/10.1073/pnas.0904089106

Pfurtscheller, G., Stancák, A., & Neuper, C. (1996). Event-related synchronization (ERS) in the alpha band — an electrophysiological correlate of cortical idling: A review. *International Journal of Psychophysiology*, *24*(1-2), 39–46. https://doi.org/10.1016/S0167-8760(96)00066-9

Poil, S.‐S., Hardstone, R., Mansvelder, H. D., & Linkenkaer-Hansen, K. (2012). Critical-state dynamics of avalanches and oscillations jointly emerge from balanced excitation/inhibition in neuronal networks. *The Journal of Neuroscience*, *32*(29), 9817–9823. https://doi.org/10.1523/JNEUROSCI.5990-11.2012

Ponce-Alvarez, A., Jouary, A., Privat, M., Deco, G., & Sumbre, G. (2018). Whole-Brain Neuronal Activity Displays Crackling Noise Dynamics. *Neuron.* Advance online publication. https://doi.org/10.1016/j.neuron.2018.10.045

Priesemann, V., Munk, M. H. J., & Wibral, M. (2009). Subsampling effects in neuronal avalanche distributions recorded in vivo. *BMC Neuroscience*, *10*, 40. https://doi.org/10.1186/1471-2202-10-40

Priesemann, V., Valderrama, M., Wibral, M., & van Quyen, M. (2013). Neuronal avalanches differ from wakefulness to deep sleep--evidence from intracranial depth recordings in

humans. *PLoS Computational Biology*, *9*(3), e1002985. https://doi.org/10.1371/journal.pcbi.1002985

R Core Team. (2018). R: A language and environment for statistical computing: R Foundation for Statistical Computing, Vienna, Austria. Retrieved from URL https://www.R-project.org/

Rahn, E., & Basar, E. (1993). Enhancement of Visual Evoked Potentials by Stimulation During Low Prestimulus Eeg Stages. *International Journal of Neuroscience*, *72*(1-2), 123–136. https://doi.org/10.3109/00207459308991629

Renart, A., & Machens, C. K. (2014). Variability in neural activity and behavior. *Current Opinion in Neurobiology*, *25*, 211–220. https://doi.org/10.1016/j.conb.2014.02.013

Richman, J. S., & Moorman, J. R. (2000). Physiological time-series analysis using approximate entropy and sample entropy. *American Journal of Physiology. Heart and Circulatory Physiology*, *278*(6), H2039-49. https://doi.org/10.1152/ajpheart.2000.278.6.H2039

Romei, V., Brodbeck, V., Michel, C., Amedi, A., Pascual-Leone, A., & Thut, G. (2008). Spontaneous fluctuations in posterior alpha-band EEG activity reflect variability in excitability of human visual areas. *Cerebral Cortex*, *18*(9), 2010–2018. https://doi.org/10.1093/cercor/bhm229

Romei, V., Gross, J., & Thut, G. (2010). On the role of prestimulus alpha rhythms over occipito-parietal areas in visual input regulation: Correlation or causation? *The Journal of Neuroscience*, *30*(25), 8692–8697. https://doi.org/10.1523/JNEUROSCI.0160-10.2010

Sadaghiani, S., Hesselmann, G., Friston, K. J., & Kleinschmidt, A. (2010). The relation of ongoing brain activity, evoked neural responses, and cognition. *Frontiers in Systems Neuroscience*, *4*, 20. https://doi.org/10.3389/fnsys.2010.00020

Samaha, J., Iemi, L., & Postle, B. R. (2017). Prestimulus alpha-band power biases visual discrimination confidence, but not accuracy. *Consciousness and Cognition*, *54*, 47–55. https://doi.org/10.1016/j.concog.2017.02.005

Satterthwaite, F. E. (1946). An Approximate Distribution of Estimates of Variance Components. *Biometrics Bulletin*, *2*(6), 110. https://doi.org/10.2307/3002019

Sauseng, P., Klimesch, W., Gerloff, C., & Hummel, F. C. (2009). Spontaneous locally restricted EEG alpha activity determines cortical excitability in the motor cortex. *Neuropsychologia*, *47*(1), 284–288. https://doi.org/10.1016/j.neuropsychologia.2008.07.021

Schaworonkow, N., Blythe, D. A. J., Kegeles, J., Curio, G., & Nikulin, V. V. (2015). Power-law dynamics in neuronal and behavioral data introduce spurious correlations. *Human Brain Mapping*, *36*(8), 2901–2914. https://doi.org/10.1002/hbm.22816

Schneidman, E., Berry II, M. J., Segev, R., & Bialek, W. (2006). Weak pairwise correlations imply strongly correlated network states in a neural population. *Nature*, *440*, 1007 EP -. https://doi.org/10.1038/nature04701

Sethna, J. P., Dahmen, K. A., & Myers, C. R. (2001). Crackling noise. *Nature*, *410*, 242 EP -. https://doi.org/10.1038/35065675

Shew, W. L., & Plenz, D. (2013). The functional benefits of criticality in the cortex. *The Neuroscientist*, *19*(1), 88–100. https://doi.org/10.1177/1073858412445487

Shriki, O., Alstott, J., Carver, F., Holroyd, T., Henson, R. N. A., Smith, M. L. [Marie], . . . Plenz, D. (2013). Neuronal avalanches in the resting MEG of the human brain. *The Journal of Neuroscience*, *33*(16), 7079–7090. https://doi.org/10.1523/JNEUROSCI.4286-12.2013

Tadel, F., Baillet, S., Mosher, J. C., Pantazis, D., & Leahy, R. M. (2011). Brainstorm: A user-friendly application for MEG/EEG analysis. *Computational Intelligence and Neuroscience*, *2011*, 879716. https://doi.org/10.1155/2011/879716

Tagliazucchi, E., Wegner, F. von, Morzelewski, A., Brodbeck, V., Jahnke, K., & Laufs, H. (2013). Breakdown of long-range temporal dependence in default mode and attention networks during deep sleep. *Proceedings of the National Academy of Sciences of the United States of America*, *110*(38), 15419–15424. https://doi.org/10.1073/pnas.1312848110

Theiler, J., Eubank, S., Longtin, A., Galdrikian, B., & Doyne Farmer, J. (1992). Testing for nonlinearity in time series: the method of surrogate data. *Physica D: Nonlinear Phenomena*, *58*(1-4), 77–94. https://doi.org/10.1016/0167-2789(92)90102-S

Van Diepen, R. M., Foxe, J. J., & Mazaheri, A. (2019). The functional role of alpha-band activity in attentional processing: The current zeitgeist and future outlook. *Current Opinion in Psychology*, *29*, 229–238. https://doi.org/10.1016/j.copsyc.2019.03.015

Vanrullen, R., Busch, N. A., Drewes, J., & Dubois, J. (2011). Ongoing EEG Phase as a Trial-by-Trial Predictor of Perceptual and Attentional Variability. *Frontiers in Psychology*, *2*, 60. https://doi.org/10.3389/fpsyg.2011.00060

Waterstraat, G., Fedele, T., Burghoff, M., Scheer, H.‐J., & Curio, G. (2015). Recording human cortical population spikes non-invasively--An EEG tutorial. *Journal of Neuroscience Methods*, *250*, 74–84. https://doi.org/10.1016/j.jneumeth.2014.08.013

Wikström, H., Huttunen, J., Korvenoja, A., Virtanen, J., Salonen, O., Aronen, H., & Ilmoniemi, R. J. (1996). Effects of interstimulus interval on somatosensory evoked magnetic fields (SEFs): A hypothesis concerning SEF generation at the primary sensorimotor cortex. *Electroencephalography and Clinical Neurophysiology/Evoked Potentials Section*, *100*(6), 479–487. https://doi.org/10.1016/S0168-5597(96)95688-9

Yu, S., Ribeiro, T. L., Meisel, C., Chou, S., Mitz, A., Saunders, R., & Plenz, D. (2017). Maintained avalanche dynamics during task-induced changes of neuronal activity in nonhuman primates. *ELife*, *6*. https://doi.org/10.7554/eLife.27119

Zhao, L., Li, W., Yang, C., Han, J., Su, Z., & Zou, Y. (2017). Multifractality and Network Analysis of Phase Transition. *PloS One*, *12*(1), e0170467. https://doi.org/10.1371/journal.pone.0170467

Zrenner, C., Desideri, D., Belardinelli, P., & Ziemann, U. (2017). Real-time EEG-defined excitability states determine efficacy of TMS-induced plasticity in human motor cortex. *Brain Stimulation.* Advance online publication. https://doi.org/10.1016/j.brs.2017.11.016